Total electron content (TEC) variability at Los Alamos, New Mexico: A comparative study: FORTE-derived TEC analysis

Zhen Huang and Robert Roussel-Dupré

Atmospheric, Environmental and Climatic Dynamics Group, Earth and Environmental Sciences Division, Los Alamos National Laboratory, Los Alamos, New Mexico, USA

Received 25 October 2004; revised 22 March 2005; accepted 27 June 2005; published 19 November 2005.

[1] Data collected from Fast On-Orbit Recording of Transient Events (FORTE) satellite–received Los Alamos Portable Pulser (LAPP) signals during 1997–2002 are used to derive the total electron content (TEC) at Los Alamos, New Mexico. The LAPP-derived TECs at Los Alamos are analyzed for diurnal, seasonal, interannual, and 27-day solar cycle variations. Several aspects in deriving TEC are analyzed, including slant to vertical TEC conversion, quartic effects on transionosperic signals, and geomagnetic storm effects on the TEC variance superimposed on the averaged TEC values.

Citation: Huang, Z., and R. Roussel-Dupré (2005), Total electron content (TEC) variability at Los Alamos, New Mexico: A comparative study: FORTE-derived TEC analysis, *Radio Sci.*, *40*, RS6007, doi:10.1029/2004RS003202.

1. Introduction

1.1. Overview of Total Electron Content Variability

[2] The ionospheric total electron content (TEC) is characterized by spatial and temporal variations that can be traced primarily to changes in solar radiation with time and geographic location, and to solar/magnetic activity. The spatial variations generally correspond to the various ionospheric latitude zones. A major maximum is at low latitudes (the tropical zone) and a secondary maximum is at the poles (the auroral zone), and TEC is a minimum at midlatitudes. The highest TEC values on the entire globe occur in the near equatorial region extending to about 20° on either side of the magnetic equator, with the peak TECs found in the equatorial anomaly region at ~15° from the magnetic equator. The temporal variations are characterized by cyclic variability on diurnal, seasonal, interannual, and 27-day solar cycle timescales.

[3] In the absence of solar/magnetic storm activity, it is the solar EUV radiation that controls temporal variability in the ionosphere. The two major solar-controlled temporal variabilities are the diurnal cycle over the 24-hour period between daytime and nighttime and the interannual cycle over the 11-year period between high and low solar activities. The diurnal cycle for TEC is such that the maximum occurs two hours after solar noon and the minimum before dawn. The seasonal variability of TEC is relatively small in amplitude, which shows a semiannual cycle with higher values at equinox and lower values at solstice. Although the solar control clearly dominates the cyclic TEC variability, ionospheric disturbance effects can lead to considerable random day-to-day variations in TEC.

[4] Many observational and experimental studies have been done on the temporal variability of ionospheric TEC on diurnal, seasonal and interannual timescales providing us with insights into detailed and specific ionospheric temporal characteristics and quantitative relationships with controlling factors. Some interesting findings include the long-term relationship between TEC and solar activity, the seasonal dependence of the time for daytime peak TEC, and the nighttime secondary TEC peak. It has been indicated that the ionospheric TEC long-term variability statistically correlates with the 11-year cycle of solar activity in the normal range [*Gordienko and Mukasheva*, 2001]. A high degree of correlation was found between the TEC and solar irradiance index $F_{10.7}$ in the range of 80–150. For $F_{10.7}$ in the range of 150–200 or less than 80, the TEC level remains virtually unchanged. It has been found that the occurrence time for the daytime TEC peak is seasonally dependent in the equatorial anomaly regions [*Tsai et al.*, 2001]. The TEC peaks are fully developed around midday in winter, early afternoon in equinoxes and late afternoon in summer. In addition to the major daytime TEC peak, a prominent secondary peak after sunset has been reported normally happening before midnight and is more pronounced around equinoxes during high solar activity at equatorial regions [e.g., *Wan Hassan et al.*, 2002]. At midlatitudes the nighttime TEC increases because of anomalous increases in the

0048-6604/05/2004RS003202$11.00

nighttime *F*2 region, a fact that has been investigated and established by many researchers since mid-1960s [e.g., *Arendt and Soicher*, 1964].

[5] The day-to-day transient TEC variations have also been investigated as an important part of the ionospheric temporal variability. One of the basic understandings on the contributing factor to the day-to-day TEC variations is the solar radiation change. It has been pointed out that day-to-day TEC variations react very sensitively to solar radiation changes. For example, correlation analysis on ionospheric response to solar radiation changes over the European area indicated a delay of up to 3 days depending on geomagnetic conditions [*Jakowski et al.*, 2002]. Examination of the ionospheric responses to the solar eclipse on 11 August 1999 found significant reductions of TEC following the turn off and on of the solar radiation with a delay of up to 40 min [*Jakowski et al.*, 2002]. Previous researches also described how the day-to-day TEC variations are related to the phases of diurnal cycle and the latitudinal location. The TEC structure at Anchorage, Alaska (61.04°N, 149.75°W) was examined for the period just following the minimum phase of solar cycle 21 and the results indicated virtually uniform TEC structure from day to day during the buildup and decay diurnal phase of the local ionosphere and pronounced day-to-day variations during the maximum and minimum of the diurnal phase [*Soicher*, 1985]. The TEC relative variability, a measure for day-to-day TEC variations, was investigated for three South American stations (Arequipa, Peru: close to the magnetic equator; Santiago, Chile: close to the southern crest of the anomaly; and Rio Grande: at midlatitudes). At the equatorial station the TEC changes from 35% during day to a peak of 60% before sunrise. At the midlatitude station the TEC changes from 30% during daytime to a dawn peak of about 50%. The TEC variations are uniform at about 50% for day and night at the crest station [*Mosert de Gonazalez and Radicella*, 1995]. The day-to-day TEC variations are relatively small at the midlatitudes.

1.2. Data Types for Characterizing TEC

[6] To characterize ionospheric TEC, there are different types of ionospheric data available. Each type of data provides a limited view of the ionosphere. On the other hand, each type of data has its particular advantages. For example, ground ionosonde station measurements provide data up to the peak of the ionosphere. Satellite-borne in situ sensors provide information near the peak and above. The observations of the Faraday rotation of radio signals from geostationary satellite beacons have limited geographical coverage while providing good time resolution. The polar orbiting satellites, such as the Navy Satellite Navigation System, provide electron content up to 1000 km (the height of the satellite) at approximately fixed time. The combination of the geostationary and polar-orbiting satellites data yields information on the spatial and temporal variation of TEC [e.g., *Davies et al.*, 1979].

[7] The most widely used data type is the TEC measurements using the Global Positional System (GPS). The GPS has a large number of satellites and monitoring stations and can present global coverage of integral electron content up to the satellite altitude of 20,200 km. Global ionosphere TEC maps are generated on a daily basis since 1995 using data from the International GPS Service tracking network, which include dense GPS ground sites on continents but very sparse stations on islands over oceans [e.g., *Schaer et al.*, 1996]. GPS provides global coverage on the topside electron content that is not available from ionosondes. It has been demonstrated that it is possible to reconstruct electron density profile and TEC in regions where ionosonde data are not available by combining ground GPS observations and relatively far ionosonde data [*Garcia-Fernandez et al.*, 2003]. However, a number of technical considerations have been addressed for the uncertainties in GPS TEC measurements [*Doherty and Klobuchar*, 1992]. Such considerations include antenna characteristics, receiver delay variations, multipath, and the environment and maintenance of an individual receiver, which should be regularly and appropriately calibrated. It has been indicated that the limit of accuracy of GPS TEC is a few TECU, which is generally tenth of TEC value for most ionospheric conditions [*Davies and Hartmann*, 1997].

[8] Empirical ionospheric models have also been developed for characterizing TEC. For example, the Bent model was developed to describe the global ionosphere for a given location, time, and date by fitting a theoretical electron density profile to a database of ionospheric measurements [*Bent and Llewellyn*, 1973]. Efforts at building a standard empirical model (the IRI model) were initiated in the late sixties and the IRI model has been developed and evolved over the years and several steadily improved editions of the model have been released. Both the Bent model and the IRI model provide average TEC values for magnetically quiet conditions while the IRI model showed better results than the Bent model in comparison with data which could be attributed to the more detailed representation of the bottomside density structure in the IRI model [*Bilitza et al.*, 1988; *Bilitza*, 2001].

[9] All the empirical models are climatic or synoptic in nature. These models provide a reasonably accurate description of the gross behavior of the ionosphere in terms of spatial and temporal features. However, they are not capable of providing the absolute ionospheric parameters with acceptable accuracies due to inadequate information about the instantaneous or local driving forces. In particular, model performances are poor during geomagnetic disturbances.

[10] The topside sounding technique provides invaluable data during various solar activity periods in different latitude regions [*Pulinets and Benson*, 1999] to improve ionospheric models and enhance our ability to extract accurate TEC from models. The topside ionosphere modeled by IRI is not adequate because of a lack of data, especially for periods of high solar activity. The Alouette and ISIS topside sounder data have been used to improve the IRI topside profile [*Bilitza et al.*, 1998; *Bilitza and Williamson*, 2000]. As considerable amount of topside sounder data has become available from the Russian Intercosmos-19 mission and other satellite borne topside sounders, a merging of these data sets and modeling approaches should lead to a reliable new topside model for the next version of the IRI model [*Pulinets et al.*, 2002].

1.3. Scope of This Study

[11] This study presents results of our comparative study on the TEC cyclic variability at Los Alamos, New Mexico on diurnal, seasonal, interannual, and 27-day solar cycle timescales for the period of 1997–2002. In this paper, the characteristics of the TEC cyclic variability during the period of 1997–2002 derived from FORTE-received Los Alamos Portable Pulser (LAPP) signals are used as a basis to characterize the TEC variability at Los Alamos. In another paper (Z. Huang and R. Roussel-Dupré, Total electron content (TEC) variability at Los Alamos, New Mexico: Comparisons with other TEC sources, submitted to *Radio Science*, 2005, hereinafter referred to as Huang and Roussel-Dupré, submitted manuscript, 2005), other TEC sources from GPS measurements, ionosonde observations, and IRI model predictions are used for comparative studies. Knowledge from such a TEC comparative study are useful in developing better tools for data calibration and characteristic recognition of the midlatitude ionosphere at Los Alamos as well as in evaluating and applying the site ionospheric corrections for communication system models.

2. Data, Theory, and Algorithm

2.1. FORTE Satellite and LAPP Transmitter

[12] The Fast On-Orbit Recording of Transient Events (FORTE) satellite was launched on 29 August 1997 by a Pegasus launch vehicle. It is in a circular, 800-km-altitude orbit inclined 70° from the Earth's equator and covers equatorial regions and midlatitudes. FORTE carries a suite of instruments, including an advanced radio frequency (RF) impulse detection and characterization experiment to measure electromagnetic pulses within a noise environment dominated by continuous wave carriers such as TV and FM stations.

[13] The FORTE radio payload is a set of tunable wideband radio receivers followed by fast digitizers. The first type of receiver operates with a bandwidth of 22 MHz, referred to as twenty megahertz and twelve bit receivers (TATRs). The second type of receiver operates with a 90 MHz bandwidth, referred to as hundred megahertz receivers (HUMRs). Both receivers are tunable across the 30–300 MHz band. One of the purposes for the radio payload is to provide data on the propagation of wideband radio signals through the ionosphere. Such data can be used to study ionospheric properties, such as changes in TEC, which produces variations in the amount of dispersion of a transient broadband RF signal. Detailed descriptions can be found in work by *Jacobson et al.* [1999].

[14] The wideband RF signals are produced by an electromagnetic pulse generator coupled to a 30 m dish/antenna, the Los Alamos Portable Pulser (LAPP). The LAPP is located at Los Alamos, New Mexico (35.872°N, 106.327°W, elevation 2274.08 m). It provides high power signals launched with high-accuracy timing and can be used to calibrate RF broadband satellite receivers. The useful bandwidth of the LAPP pulse extends from below 30 MHz to above 200 MHz. The frequency components of the nearly impulsive signals produced by LAPP are dispersed as they pass through the ionosphere and are received by a set of crossed, nadir pointing, log periodic antennas on the FORTE satellite. The signals are band pass filtered and digitized and transmitted back to a ground station for processing and archiving.

2.2. FORTE-LAPP Event Data Description

[15] This work uses FORTE received LAPP VHF signal data. A LAPP signal subdatabase has been created by searching through the FORTE database for the LAPP events, which occurred when the FORTE satellite was within a range of slant distance of 3500 km from the center of Los Alamos. The generated subdatabase includes over 2200 LAPP events covering a period from 1 November 1997 to 11 July 2002. The LAPP events mostly occur during daytime. Fortunately, extensive operations were also conducted into nighttime during the year of 1998, offering a possibility to investigate a full cycle of diurnal variations. Figures 1a and 1b show the geographical location of the subsatellite point and the ionospheric pierce point at 350 km, respectively. Figure 1c gives the temporal coverage for all the events in the LAPP signal subdatabase used in this study.

[16] The LAPP signal subdatabase consists of two types of time series data: one type is from the HUMR receiver, sampled at 300 megasamples/s, and the other type is from the smaller frequency band of TATR receivers, sampled at 50 megasamples/s. Both HUMR and TATR data are available before October 1999 and only HUMR data is available after then, that is, when the TATR receiver failed. Figures 2a and 2b and Figures 3a

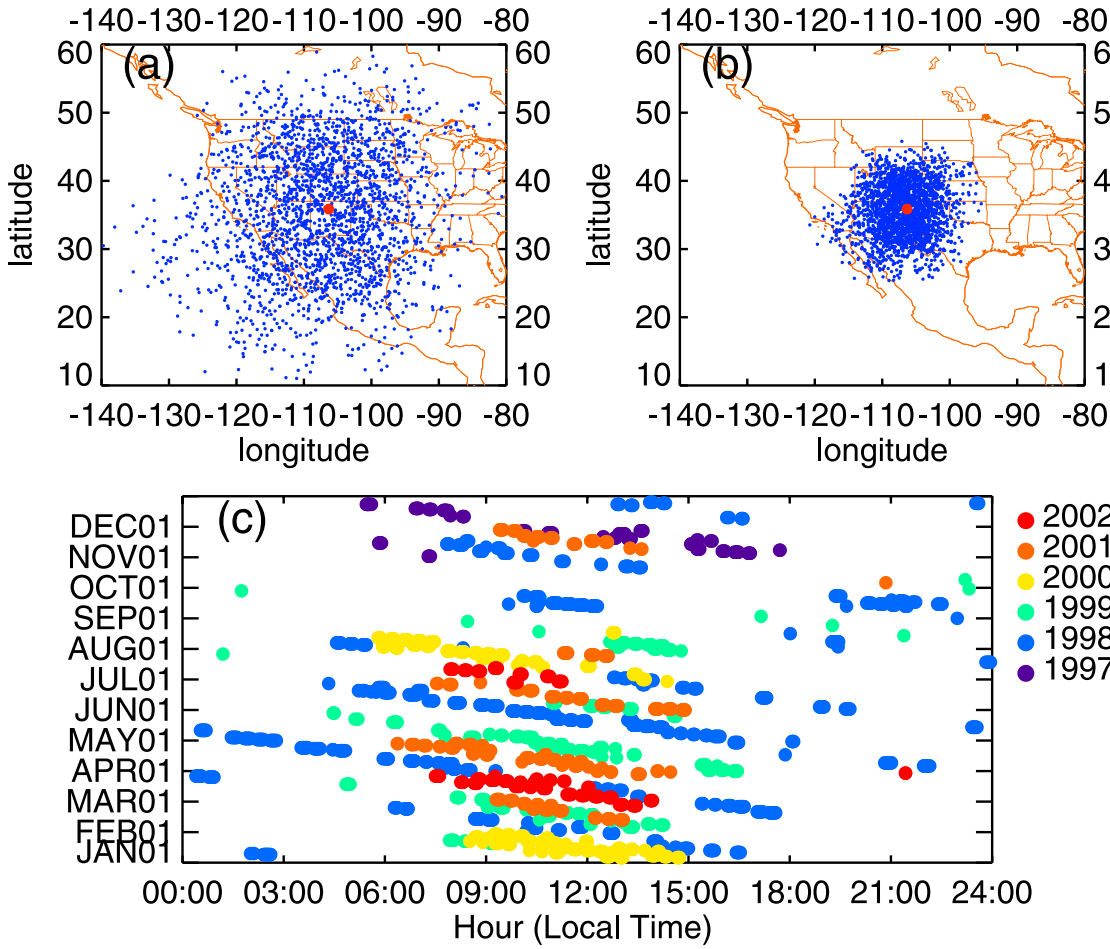

Figure 1. Spatial distribution and temporal occurrence of FORTE-received LAPP events: (a) geographical location of the subsatellite point; (b) geographical location of the ionospheric pierce point at 350 km; and (c) year, date, and time of day distribution during the data period of 1997–2002.

and 3b show an example of a FORTE-received LAPP signal and its spectrogram from the HUMR and the TATR receiver, respectively. Figures 2 and 3 illustrate several factors that affect the appearance of the received signal. Because of the differences in the slant distance between the receiver and the transmitter, signal-to-noise ratio, time of day, and solar activity, the received signal and its spectrogram show noticeably different "chirps." In the case of the TATR sample signal (Figure 2), its spectrum is less "chirped" because of the low solar activity in 1998 and relatively shorter slant distance compared to the HUMR sample signal (Figure 3), where solar activity is high in 2001 and the slant distance is much longer.

2.3. Radio Wave Propagation Theory

[17] The free electrons that populate the Earth's ionosphere are responsible for the "propagation effects" observed in the radio waves that penetrate the ionosphere. The total electron content (TEC), that is, the number of free electrons per unit volume integrated along the ray path to the receiver, is the most important descriptive quantity that characterize these effects.

[18] The dispersion of an impulsive radio wave traversing the ionosphere arises because the different frequency components that make up the temporal structure of the pulse propagate at different speeds owing to the interaction of the electromagnetic wave field with the free electrons. Above the plasma resonance frequency (generally below 20 MHz in the ionosphere), this interaction reduces with increasing frequency ($\sim 1/f^2$). The net effect upon radio waves is proportional to the TEC along the line-of-sight signal path from a transmitter to a receiver. At VHF (30–300 MHz), and in the GPS L band, or even higher, this effect is significant. Therefore

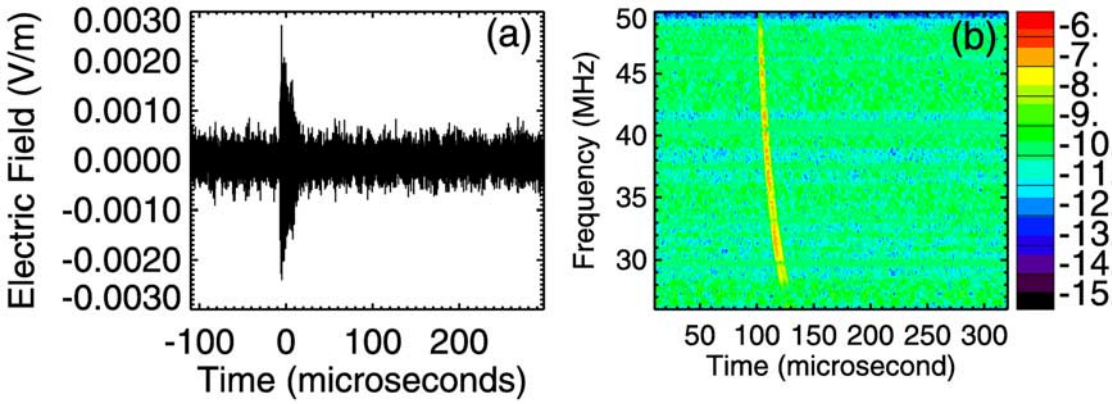

Figure 2. TATR signal (a) time series and (b) spectrogram for FORTE-received LAPP event on 4 May 1998, 2250:00.004628 UT, for FORTE location 29.4912°N, 114.943°W, 836.5 km.

TEC is a key parameter that describes the major impact of the ionized atmosphere on the propagation of radio waves. An algorithm for TEC estimation can be developed from the differential phases of transionospheric radio signals at two frequencies, as for GPS dual frequencies, or over a broadband of VHF frequencies, as in the case of this study.

[19] Radio waves traveling through the ionosphere are dispersed because of the ionospheric electron content. The ionosphere is birefringent because the Earth's magnetic field also separates an incident pulse into two modes, each propagating at a different speed. At VHF frequencies, the net effect on the signal delay, τg, can be written as a function of frequency, f [*Massey et al.*, 1998],

$$\tau g = \tau 0 + \alpha Ne/(f + fc\cos(\beta))^2 + O(fp/f)^4, \quad (1)$$

where $\tau 0$ is vacuum accumulated temporal delay along the slant path, $\alpha = 1.34 \times 10^7$ when all quantities are expressed in *mks* units, and *Ne* is the total integrated density of electrons along the path, β is the angle between the wave vector and the magnetic field, and *fc* is the electron cyclotron frequency. The $1/f^2$ term is due to the effects of the integrated electron density along the slant path (TEC effects). The $1/f^4$ term is a correction associated with higher-order integral moments of the electron density and refractive bending (quartic effects).

[20] For each frequency, equation (1) can be written as

$$\Delta t = \tau g - \tau 0 = F_{tec}(f^{-2}) + F_{mag}(\beta, f) + F_{qrt}(f^{-4}), \quad (2)$$

where the subscript *tec*, *mag*, and *qrt* denotes a function related to TEC effects, magnetic field effects, and quartic effects, respectively. Equation (2) will be used as the

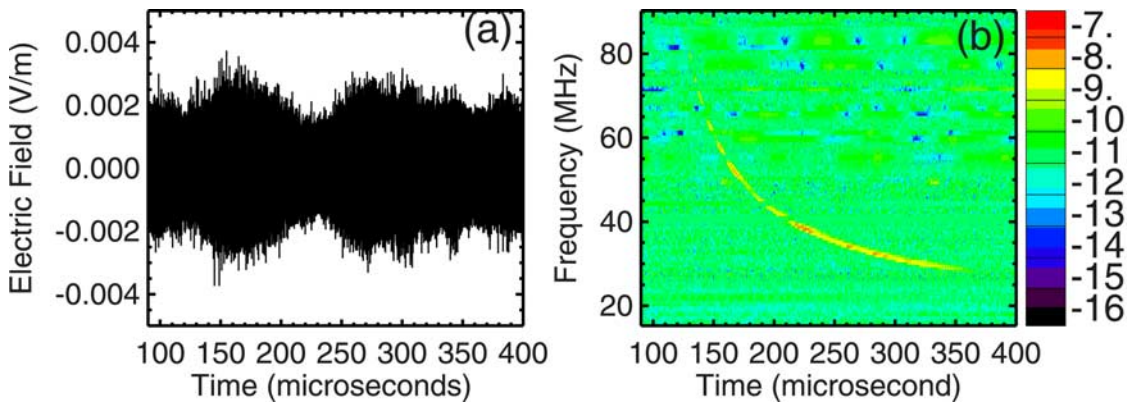

Figure 3. HUMR signal (a) time series and (b) spectrogram for FORTE-received LAPP event on 26 February 2002, 2002:01.000000 UT, for FORTE location 47.7817°N, 107.952°W, 803.960 km.

Table 1. Event Elevation Distributions

Elevation Angle, deg	All Time, %	Daytime, %	Nighttime, %
<20	7.1	5.9	11.4
20–30	26.4	25.9	29.8
30–40	26.8	28.7	23.5
40–50	17.0	18.4	14.3
50–60	10.8	11.0	10.8
>60	9.7	9.9	9.9

theoretical basis on which an algorithm for deriving the slant TEC and other ionospheric properties is developed from FORTE-received LAPP signal data. The coefficients of these terms represent various characteristics of the ionosphere [*Roussel-Dupré et al.*, 2001].

2.4. Algorithm for Deriving Total Electron Content (TEC)

[21] In order to derive slant TEC from a FORTE-received LAPP signal, we developed a signal analysis algorithm. This algorithm is based on the relationship between frequency and the three effect functions given in equation (2), F_{tec}, F_{mag}, and F_{qrt}, and combines sliding window FFT and curve fitting techniques along with carrier-suppressing and slow-mode removal. The sliding window FFT technique is used to obtain signal spectrograms. A Gaussian curve fit is used to determine the arrival time of peak power for each frequency window of a signal spectrogram. Polynomial curve fits are applied to peak power profiles to get coefficients for deriving TEC and quartic term corrections. See Appendix A for a step-by-step description of the algorithm.

[22] The slant TECs derived using the algorithm are converted to vertical TECs for this study. It has been indicated that a simple "plane-parallel" model describes the FORTE-derived slant TEC very well during daytime and nighttime for elevation angle greater than 20° [*Tierney et al.*, 2001]. In the "plane-parallel" model, the vertical TECs are modeled as the slant TEC multiplied by sinθ, where θ is the elevation angle. The elevation angle is measured between a line tangent to the surface of the Earth and a line joining the LAPP location and the FORTE satellite. The smaller the elevation angle is, the greater the slant distance of the ray path from LAPP to FORTE. Table 1 gives elevation angle distributions for the FORTE-LAPP event data used in this study. It shows that those events with elevation angles less than 20° account for about 6% of the total events during daytime (0700–1900) and 11% during nighttime (1900–0700). In converting slant TEC to vertical TEC, we use the "plane-parallel" model unless it is otherwise indicated.

[23] The algorithm is applied to both TATR and HUMR signals. Given the different bandwidths for the TATR (22 MHz) and HUMR (90 MHz), we investigated whether this algorithm can be applied to both types of signal consistently without getting biased TECs toward either type of signal. Since there were no TATR and HUMR overlapping observations at a given event time, we use hourly averages for comparisons. Figure 4a and Figure 4b compare the hourly averaged TECs derived from the TATR and that derived from the HUMR for all the available data during the overlapping period of time (1997–1999) for January–April and for September–December, respectively (May–August data are too sparse to do comparisons). We can see that although the differences between the TATR-derived TECs and

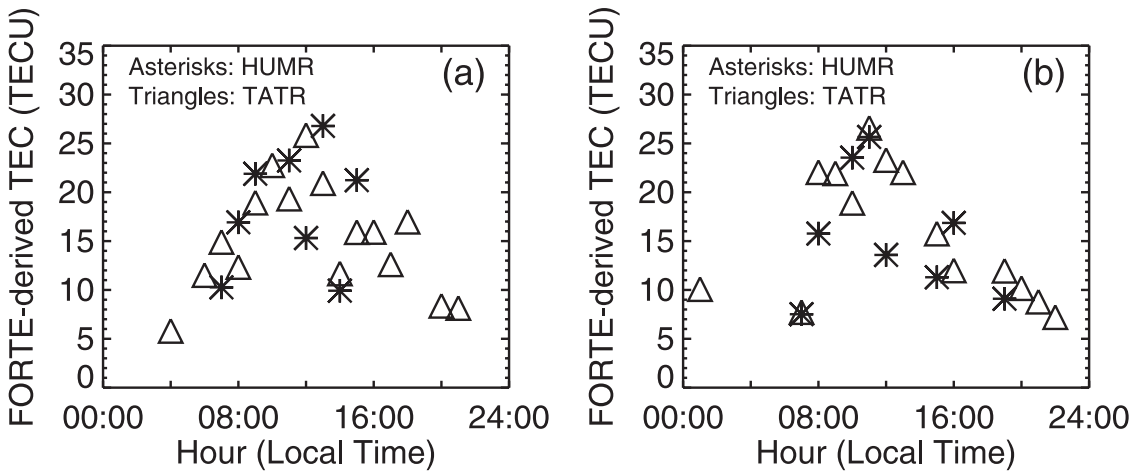

Figure 4. Comparisons in FORTE-derived TEC from TATR and HUMR receivers, averaged for (a) January–April and (b) September–December.

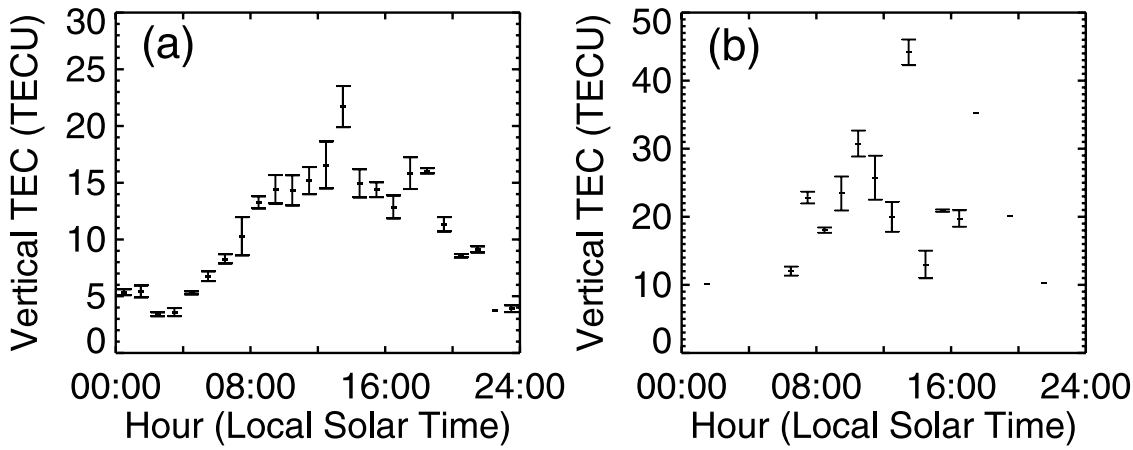

Figure 5. FORTE-derived TEC diurnal cycle, annual averaged hourly means, and standard deviations for (a) 1997–1998 and (b) 1999–2001.

the HUMR-derived TECs can be as large as up to 50% of the base TEC values, the results do not seem to suggest the existence of receiver-biased differences. Therefore the first three years (1997–1999) with mixed TATR and HUMR data and the second three years (2000–2002) with HUMR only data can be combined to a 6-year time series data for use in this study without receiver bias corrections required.

3. FORTE-Derived TEC Analysis

[24] In this section, we present results of FORTE-derived TEC. The FORTE-derived TECs for the period from November 1997 to July 2002 are analyzed to describe the TEC variability at Los Alamos on diurnal, seasonal, interannual, and 27-day timescales. The day-to-day TEC variations are also evaluated. Several issues regarding the uncertainties in the TEC analysis are addressed.

3.1. Variability Analysis

3.1.1. Diurnal Cycle

[25] To study diurnal variability we use the data from November 1997 to December 1998 for its relatively dense temporal coverage over a 24-hour period and more complete seasonal coverage. Figure 5a gives the annual averaged hourly TEC means and standard deviations for 1997–1998. On average, the TEC amplitude at Los Alamos displays a diurnal cycle with a minimum of about 3 TECU and a maximum up to 22 TECU for low solar activity years (1997–1998). The standard deviations of TEC annual mean are smaller than 5 TECU. The peak TEC occurs around 1300–1400 local solar time (LST). Instead of a second peak before midnight in equatorial regions, in Los Alamos we found a second peak at local solar time before sunset between 1700 and 1800.

[26] To examine possible differences in the timing and amplitude of TEC diurnal cycle for low and high solar activities, we analyzed TEC data from 1999–2001. A half diurnal cycle can be identified approximately from dawn to sunset while the other half diurnal cycle has to be estimated because of the lack of data during nighttime for these years. Figure 5b gives annually averaged hourly TEC means and standard deviations for 1999–2001.

[27] The timing of the diurnal cycle for high solar activity years is the same as that for low solar activity years. The diurnal peak TEC also occurs at 1300–1400 local solar time. Furthermore, the semidiurnal feature revealed from low solar activity years also exists for high solar activity years. The amplitude of the TEC diurnal cycle for high solar activity years changes from a low of smaller than 10 TECU (no data available at the minimum TEC time) to a high of about 44 TECU. Compared to the low solar activity years, the diurnal peak TEC is doubled at the high solar activity years. The diurnal lowest TEC was estimated to be about 6 TECU from the TEC value (10 TECU) at 0100–0200 local time (LT). Therefore the amplitude of TEC diurnal variability is much larger at high solar activity years than that at low solar activity year. The standard deviations for 1999–2001 averaged hourly TECs are also smaller than 5 TECU.

[28] Our estimates on the magnitude of the TEC diurnal cycle at Los Alamos are comparable to other midlatitude TEC studies. *Davies and Hartmann* [1997] studied the TECs at Boulder, Colorado and reported a diurnal cycle with a minimum of about 5 TECU and a maximum around 25 TECU for February in 1994 [*Davies and Hartmann*, 1997, Figure 2], a year with

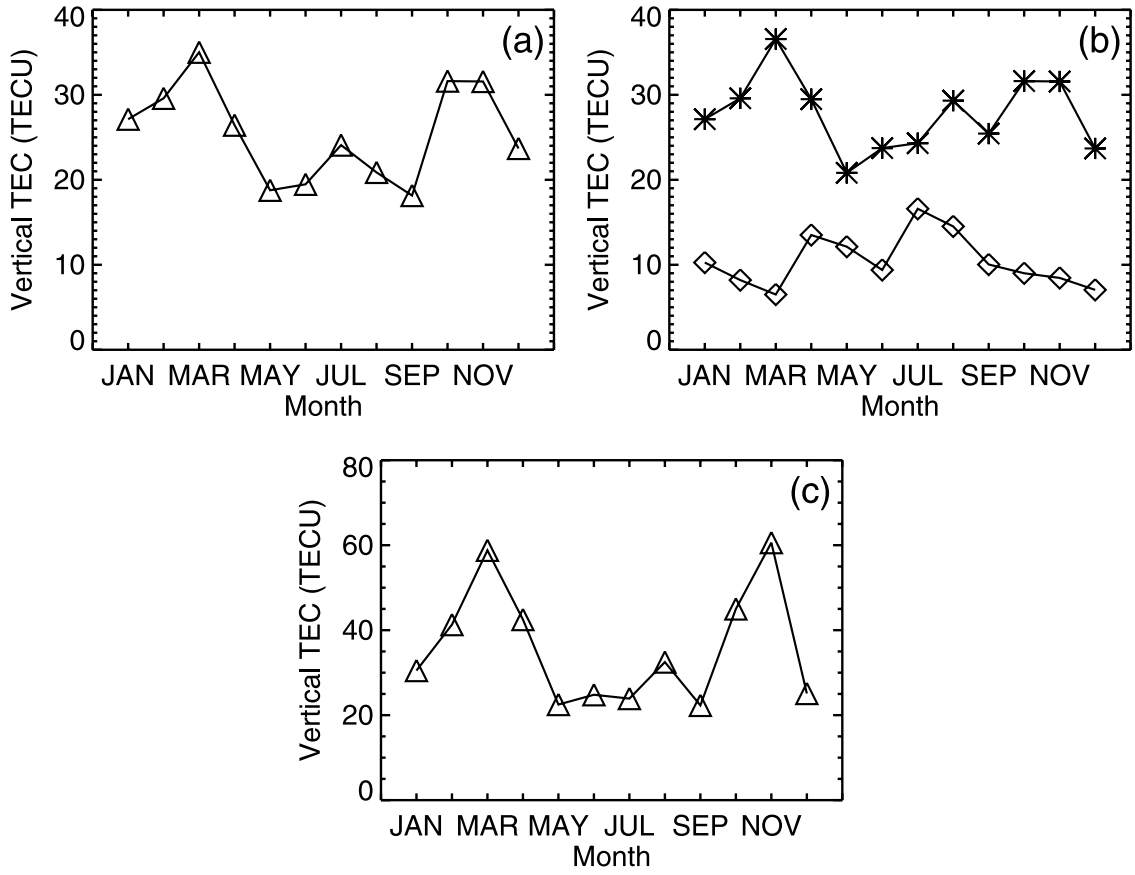

Figure 6. FORTE-derived TEC seasonal cycle for 1997–2002 averaged for (a) 24-hour, (b) daytime (0700–1800 LT) and nighttime (1800–0700 LT), and (c) peak TEC 4-hour (1000–1400 LT) periods. See text for details.

about the same solar activity strength as 1997–1998. Another midlatitude TEC study [*Ma and Maruyama*, 2002] presented results in the eastern hemisphere (35°N, 139°E) for 2001, a high solar activity year. Their analysis on the TEC variations for the selected 9 days [*Ma and Maruyama*, 2002, Figure 6] shows a diurnal cycle with minimum TEC varying from 15–20 TECU in June and August to 5–10 TECU in November and a corresponding maximum changing from 35–65 TECU to 65–90 TECU. Our results on annual averaged diurnal cycle for high solar activity years fall within their variation ranges to the lower end. Given the 15° difference in magnetic latitude (Ma and Maruyama's location is 15° closer to the magnetic equator than Los Alamos), such differences in the magnitude of the TEC diurnal cycle can be reasonably expected.

3.1.2. Seasonal Cycle

[29] The FORTE-derived TEC also displays a well-developed seasonal cycle. Figure 6a gives 1997–2002 averaged monthly mean daily TEC from January to December. It shows that monthly mean daily TEC has two peaks, one is at early spring (March) and the other is at late autumn to early winter (October–November). The lower TEC occurs in summer time from May to September. The monthly mean daily TEC varies from a minimum of about 18 TECU to a maximum of about 32 TECU, making the amplitude of seasonal variability comparable to the background TEC.

[30] To determine if there exists a day and nighttime difference in the seasonal cycle, we computed monthly mean TECs for daytime and nighttime separately. Figure 6b gives monthly TEC averaged over daytime from 0700–1800 LT (asterisks) and nighttime from 1800 to 0700 (diamonds). We found that the stronger daytime TEC dominates the seasonal cycle characteristics while the much weaker nighttime TECs do not develop a well-defined seasonal cycle. However, the nighttime monthly mean TECs seems to vary with season having an opposite phase with respect to the daytime seasonal cycle.

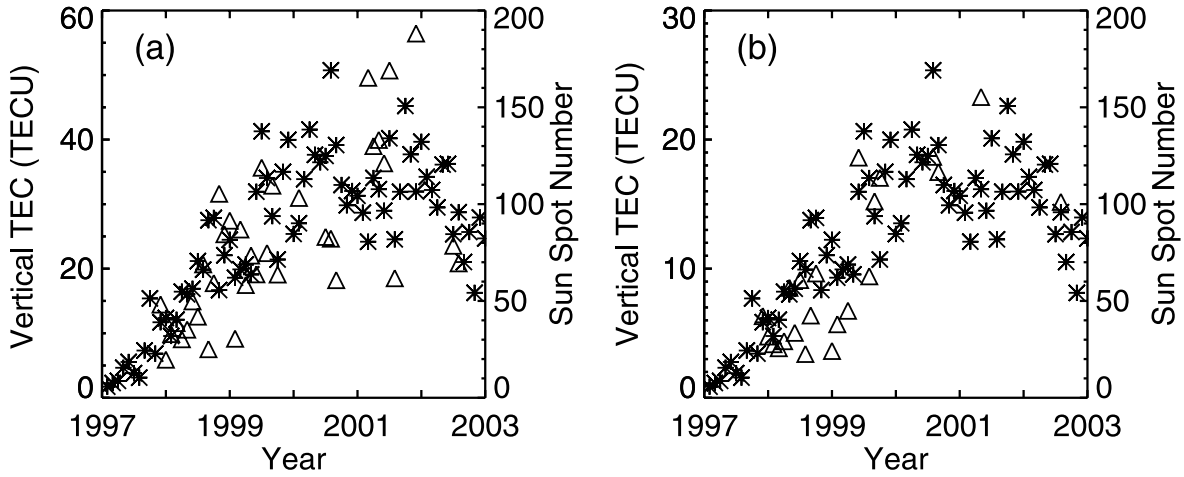

Figure 7. FORTE-derived TEC interannual variations for (a) daytime (0700–1800 LT) monthly mean TECs and (b) nighttime (1800–0700 LT) monthly mean TECs. Also shown are monthly sunspot numbers (asterisks).

[31] It has to be pointed out that the monthly averaged daily or daytime/nighttime means describe only characteristic feature of seasonal TEC cycle. Because of the TEC diurnal cycle and day-to-day fluctuations, the amplitude of the TEC cycles has been significantly smeared out. While we were not able to conduct a complete study of an hourly based TEC seasonal cycle because of a lack of data especially for nighttime, we demonstrate the effect using the seasonal cycle for the 4-hourly averaged TEC during peak TEC time (1000–1400 LT) (Figure 6c). Despite of the similar pattern of seasonal cycle, a twofold increase of the seasonal peaks (increased from 30 TECU to 60 TECU) has been found compared to what the monthly mean daily averaged TECs described and thus a much stronger amplitude of the TEC seasonal cycle during the 4-hour peak TEC time window.

3.1.3. The 11-Year Solar Cycle

[32] The TEC variability on the 11-year solar cycle has been studied for the half solar cycle from 1997 to 2002. Figures 7a and 7b show the relationships between the FORTE-derived monthly mean TEC (triangles) and the monthly mean sunspot number (asterisks) during daytime (0800–1800) and those during nighttime (1900–0700), respectively. As can be expected the TEC increases as the sunspot number increases during the half 11-year solar cycle. The TEC variability on the 11-year solar cycle scale is dramatic. During daytime, the monthly TEC varies from about 10 TECU at lowest solar years (1997–1998) to 50–60 TECU at highest solar years (2000–2001) and then begins to drop rapidly in 2002. Similarly, the monthly TEC varies from 5 TECU to 20 TECU then drops in 2002 during nighttime. Furthermore, we found that the variances of daytime monthly mean TEC superimposed on the long-term trend seem to increase as solar activity enhances through the half 11-year solar cycle. This may be indicative of the contributions due to ionospheric scintillation (to be discussed in another paper).

3.1.4. The 27-Day Solar Cycle

[33] The 27-day solar cycle results from the Sun's rotation on its axis once in about 27 days. Since the Sun is a ball of gas, it does not rotate rigidly like the solid planets do. In fact, the Sun's equatorial regions rotate faster (taking only about 24 days) than the Sun's polar regions (which rotate once in more than 30 days). This rotation was first detected by observing the motion of sunspots. By studying the position of sunspots on successive days Galileo inferred that the Sun rotates, and established its rotation period as close to one lunar month. The TEC variability associated with the 27-day solar cycle is also examined. We used daytime data for January and July of 2000, which cover more than 15 days for the given months. The nighttime case study was not possible to conduct because of a lack of data. Figures 8a and 8b show daytime TEC variability for January 2000 (averaged over 1000–1400 LT) and July 2000 (averaged over 0800–1200 LT), respectively. Also given in Figure 8 are the corresponding variations in daily sunspot number (shown as asterisks). We can clearly see the 27-day solar cycle for both months. The 27-day cycle sunspot number varies in a range from lows of 125–150 to highs of 200–280, a little smaller than a twofold increase. The 27-day solar cycle does have a signature in the daytime TEC variability. The amplitude of the 27-day TEC variability can vary from 20 TECU to 50 TECU in January and 15 TECU to 30 TECU in July, a twofold to threefold increase.

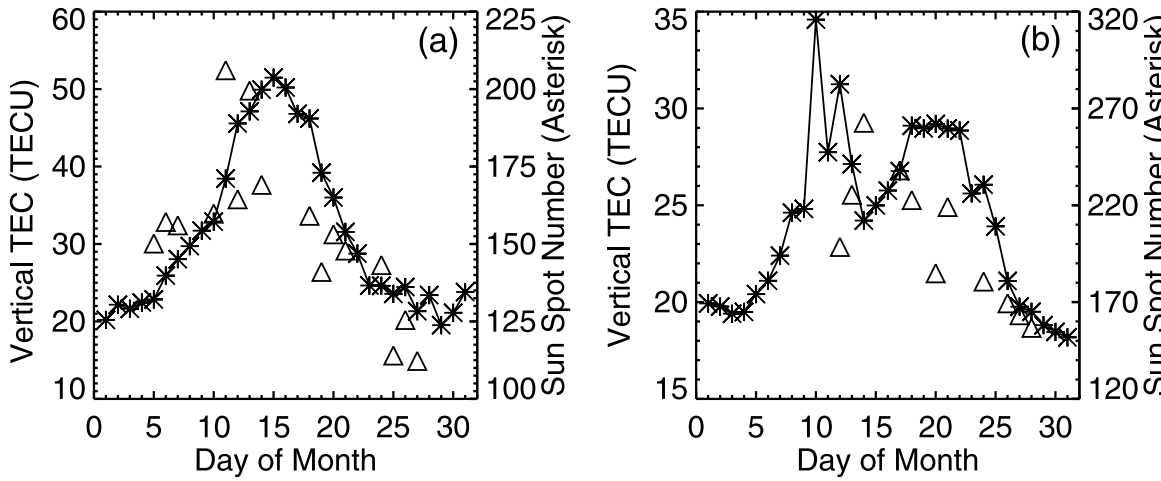

Figure 8. FORTE-derived TEC (triangles) 27-day solar cycle for (a) January 2000, averaged over 1000–1400 LT, and (b) July 2000, averaged over 0800–1200 LT. Daily sunspot numbers are shown as asterisks.

3.1.5. Day-to-Day Variations

[34] For day-to-day TEC variations, we examined the TEC relative variability (defined as the ratio of the TEC standard deviations for a given day/hour to the seasonally averaged TEC for the given hour) for the three seasonal TEC phases, at 4-month time intervals to reduce the influences from seasonal changes. Figures 9a and 9b give the TEC relative variations for January–April (pluses), May–August (asterisks), and September–December (diamonds) of low solar activity years (1997–1998) and high solar activity years (2000–2001), respectively. It has been found that the day-to-day TEC variations during low solar activity years are usually below 10% throughout the year during nighttime. During daytime TEC relative variations are small in summer months (less than 10%) while can be large in other months (up to 30%). We found that the day-to-day variations increase as the daytime TEC increases from sunrise to midday peak TEC time and that the peak day-to-day variation time is also at the TEC peak time (1300–1400 LT). Furthermore, there seems to exist a secondary day-to-day variation peak at the time from sunset to before midnight (2100–2200 LT). During high solar activity years, the daytime day-to-day TEC variations have the same magnitude as those during low solar activity years. The relative

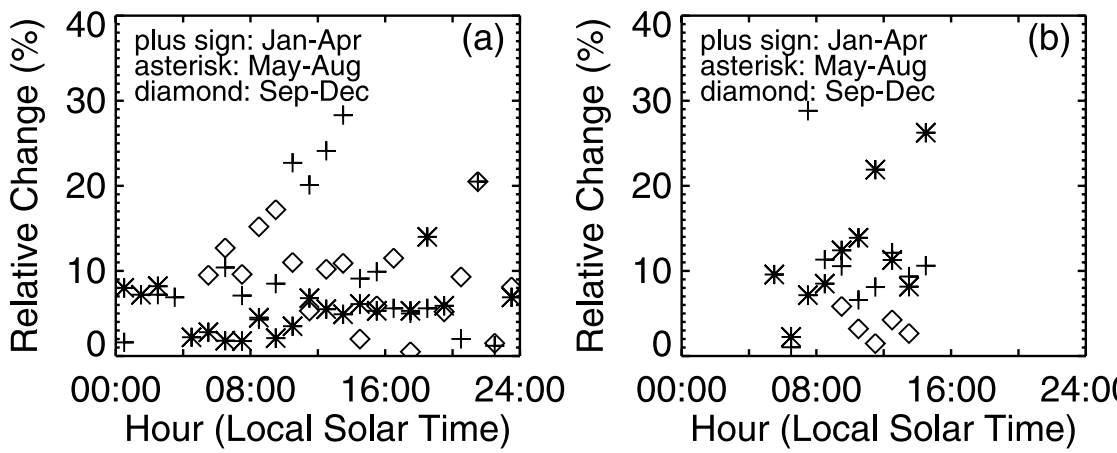

Figure 9. FORTE-derived TEC day-to-day variations and relative changes with respect to seasonal means (January–April, May–August, and September–December) for (a) low solar activity years (1997–1998) and (b) high solar activity years (2000–2001).

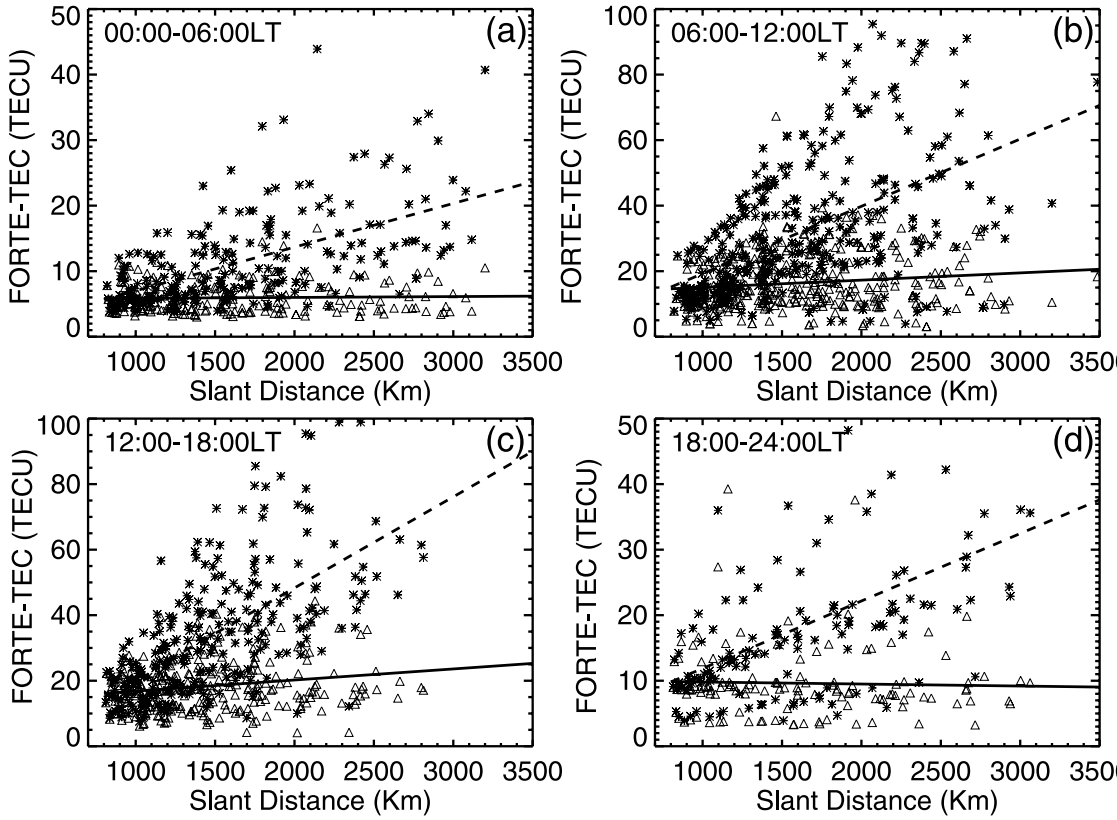

Figure 10. Slant TECs (asterisks) and vertical TECs (triangles) converted using the "plane-parallel" model and their linear curve fit (dashed line, slant TECs; solid line, vertical TECs) for (a) 0000–0600 LT, (b) 0600–1200 LT, (c) 1200–1800 LT, and (d) 1800–2400 LT.

variability is usually below 15% and sometime can reach 30%.

3.2. Uncertainty Evaluation

3.2.1. Slant to Vertical TEC Conversion

[35] In converting slant TEC to vertical TEC, this study applies the simple "plane-parallel" model to the FORTE-derived slant TEC. Because of the Earth's curvature, such a simplification can have effects on the derived vertical TECs for low elevation angles under large electron density spatial gradients [*Conker and El-Arini*, 2002]. In this section we quantitatively describe the biases from using such a simple conversion model and discuss the degree of related uncertainties in interpreting our results.

[36] To examine whether the vertical TECs derived from the simple "plane-parallel" model can be possibly biased we use the data for 1998. Figures 10a–10d demonstrate the relationship between the slant TEC and the vertical TEC derived using the "plane-parallel" model for four 6-hourly periods of time, respectively, where asterisks indicate slant TEC and triangles are the corresponding vertical TECs. We can visualize the existence of biases. During daytime (Figures 10b and 10c) there is an overestimate trend for the vertical TEC at a rate of about 2–4 TECU per 1000 km of slant distance on a background TEC of 15 TECU, making a positive bias of about 13–27% per 1000 km. During nighttime a small underestimate of up to 1 TECU is superimposed on background TEC of 10 TECU as slant distance increases to 3500 km, or a negative bias of less than 5% per 1000 km, for the time period from sunset to midnight (Figure 10d). No measurable biases can be seen for the period from midnight to sunrise (Figure 10a).

[37] The above analyses indicate that the slant distance from transmitter to the receiver can affect the derived vertical TEC depending on the time of day. Positive biases can result during daytime as the slant distance increases while very small negative biases may exist during nighttime for significantly long slant distances.

[38] To examine biases due to use of the "plane-parallel" model for active solar years, we conducted case studies for selected events given the limited data for

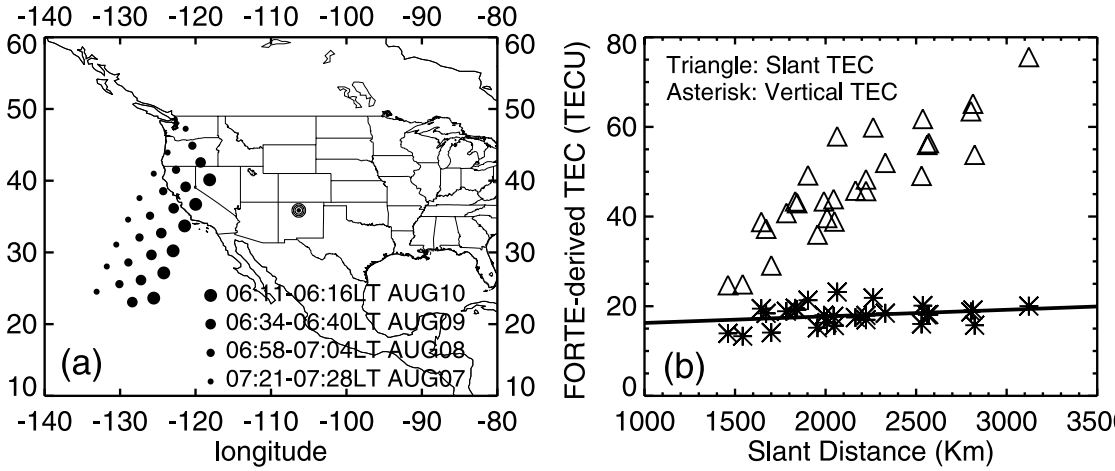

Figure 11. (a) Geographical location of the FORTE satellite. (b) Slant TECs (triangles) and vertical TECs (asterisks) derived from LAPP events during 7–10 August 2000. Solid line is the linear fit for vertical TECs.

active solar years (2000–2001). We identified an event group for an active solar year from 7 to 10 August 2000. The group consists of four consecutive day satellite overpasses and each overpass has 6–8 FORTE-recorded LAPP events. Figure 11a shows the time and location of FORTE satellite for the LAPP events. The local solar time of these events spans about one hour from 0611 to 0728. Figure 11b shows the slant TECs and the vertical TECs for these events. Positive biases at about 1.5 TECU per 1000 km are found (or about 9% of background TEC). Compared to the event-averaged 12% bias for the corresponding conditions for 1998 the results suggest that the biases for the active solar year (2000) are close to those for quiet solar year.

[39] For the worst bias case (peak TEC daytime period, 1000–1400 LT), we also selected a group of events from an active solar year (2001) for three consecutive days (21–23 February). Figure 12a shows the satellite location and time for the selected events. The event group covers three FORTE overpasses each with 6–8 FORTE recorded LAPP events. All the events occurred within one hour of time span around 1023–1116. Figure 12b shows the slant TEC and the vertical TEC for these events. The linearly fitted data line of vertical TEC

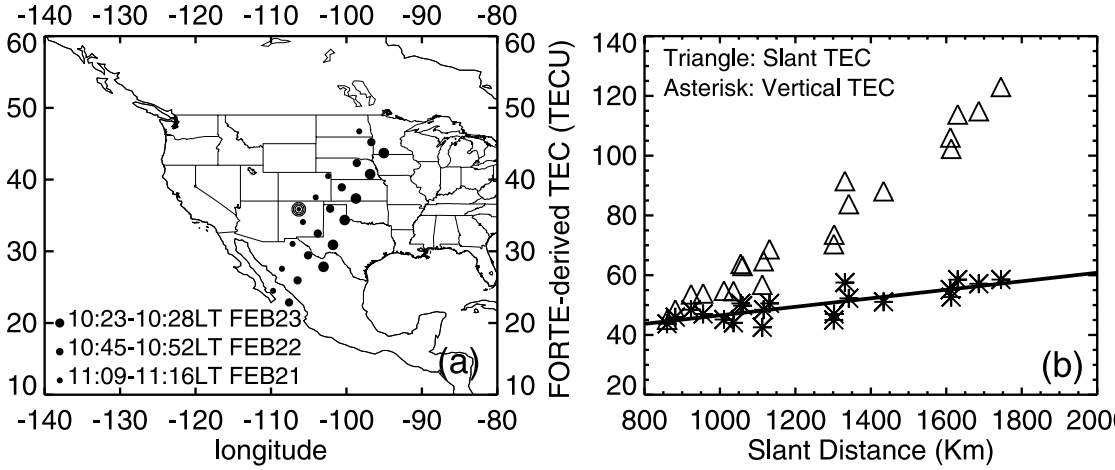

Figure 12. (a) Geographical location of the FORTE satellite. (b) Slant TECs (triangles) and vertical TECs (asterisks) derived from LAPP events during 21–23 February 2001. Solid line is the linear fit for vertical TECs.

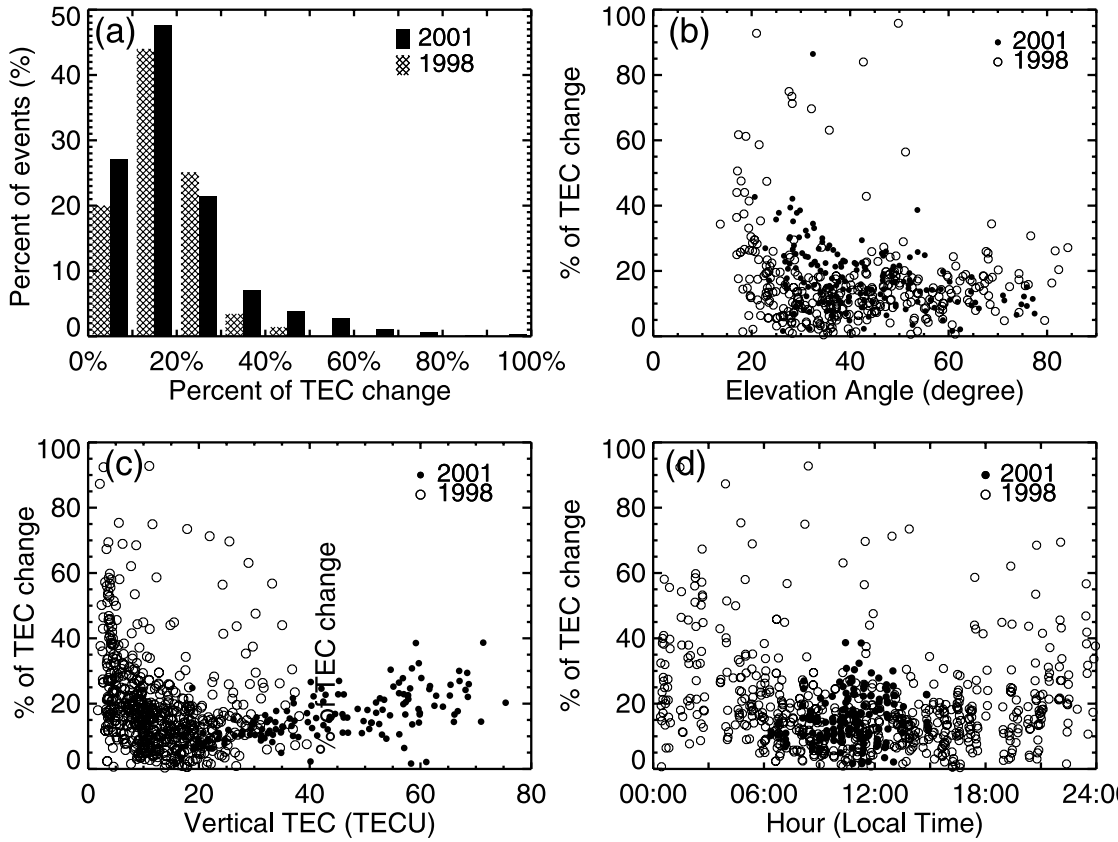

Figure 13. Quartic effects on FORTE-derived TEC for 1998 and 2001. (a) Percentage of event occurrence for relative contribution categories (0%–100%, percentage TEC changes due to quartic delay). Solid bar represents 2001 and hatched bar represents 1998. (b) Elevation angle. (c) TEC magnitude. (d) Time of day (solid circles, 2001; open circles, 1998).

suggests positive biases of about 12.5 TECU per 1000 km (or about 28% of the background TEC). Compared to the event-averaged bias for the corresponding conditions of 1998 (45%), the event-specific bias of 28% represents a reasonable example given that the maximum slant distance for the events of the 2001 case study is smaller than 2000 km instead of longer than 3000 km in the 1998 bias analysis. Regardless of the differences in absolute TEC biases, our results indicate that the relative biases with respect to background TEC at active solar years do not exceed the ones at quiet solar years.

[40] Our analysis also found that the derived vertical TECs can be affected by the direction at which the LAPP points to FORTE satellite. This is because the differences in local solar time at the FORTE location and that at the LAPP location along with the associated horizontal TEC gradients due to the diurnal cycle. Also, factors such as ionospheric spatial irregularity and scintillation in the afternoon ionosphere may play important roles. These are beyond the scope of this study and will be discussed in detail in another paper on scintillation characteristics at Los Alamos.

3.2.2. Quartic Effect

[41] It is necessary to examine the uncertainties in our FORTE TEC analysis due to ignoring the quartic term that results from refractive bending and high-order moments. To evaluate contributions of the quartic term to derived TECs, we compared slant TEC values with the quartic term included in curve fitting and those obtained by fitting a $1/f^2$ curve to the measured signal delay data for a quiet solar year (1998) and an active solar year (2001) under a variety of conditions.

[42] How often may significant quartic effects occur at Los Alamos? Figure 13a shows the percentage of event occurrences verses relative changes in TEC due to quartic effects. The majority of the events (a little less than half of the events) observed quartic term contributions to TEC in the 10% to 20% category. About 25% of the events fall in the less than 10% of the quartic term contribution category and another 25% of the

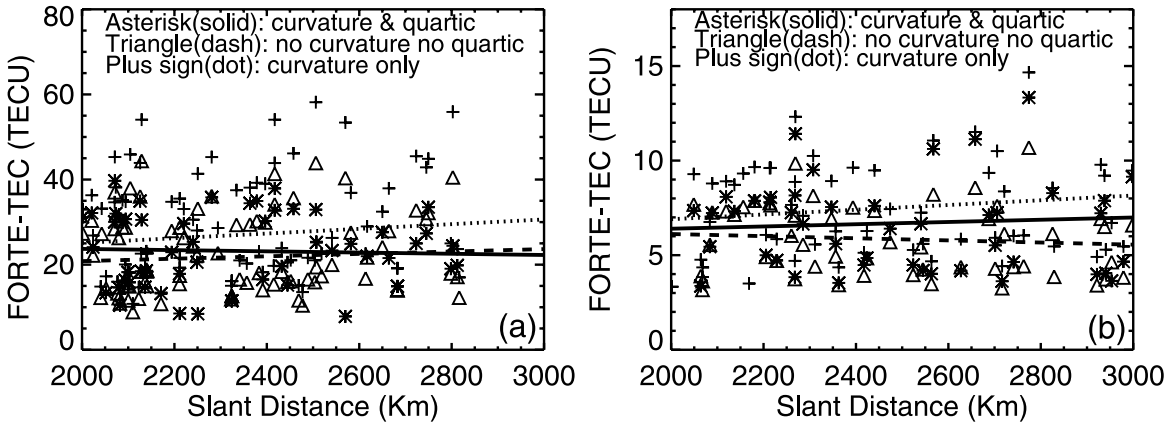

Figure 14. Curvature and quartic effects on FORTE-derived vertical TECs for (a) daytime (0800–1700 LT) 1998 and (b) nighttime (2000–0500 LT) 1998. Pluses and the dotted line represent curvature effect only, triangles and the dashed line represent no curvature and no quartic effects, and asterisks and the solid line represent inclusion of curvature and quartic effects.

events fall in the 20% to 30% of the quartic term contribution category. These three categories of events consist of over 95% of the events. Only about 5% of the events observed quartic term contributions larger than 30%. Therefore the chances for the occurrence of significant quartic effects at Los Alamos are very small and the $1/f^2$ curve fitting approximation can work well for most cases.

[43] The significance of quartic effects has been found related to the elevation angles of the slant path of a transionospheric radio wave. It has been pointed out that the quartic terms begin to have a significant effect when the elevation angles are within about 45° to the horizon and electron densities are high [*Argo et al.*, 1999]. Figures 13b and 13c give our results showing how the quartic effects change with elevation angle and vertical TEC, respectively. We found that the critical elevation angles, at which the quartic terms begin to have a significant effect, are about 30° to 40°. Beginning at the critical elevation angle, the quartic effect increases exponentially from around 10%–15% relative contributions to over 60% at the lowest possible elevation angles (about 15°). It seems that the critical elevation angle is larger (40°) at active solar year (2001), when the base TECs are relatively large, than that (30°) at quiet solar year (1998). We also found that at the TEC levels close to the base values (15–30 TECU) the quartic effects are normally small (about 10% on average) while they begin to increase linearly from less than 10% up to 30% as the TEC increases beyond the base values. On the other hand, the quartic effects increase exponentially as the TEC falls below the base values and the most significant quartic effects actually occur when TECs are very small.

[44] Our results also indicate that the most significant quartic effects occur at nighttime. Figure 13d gives the diurnal changes of the quartic effects. We can see that on average, daytime effects are 10%–20% while nighttime effects are 30–40%. Also, the magnitudes of the effects are more diversified at nighttime than those at daytime.

[45] In conclusion, significant quartic effects most possibly happen at small elevation angle (smaller than 40°), during nighttime, and at very large TEC or very small TEC conditions.

3.2.3. Multifactor Data Agreement

[46] The above evaluations of the uncertain factors in our FORTE-derived TEC analysis suggest that some improvement in agreement with data may be obtained in a more detailed study. In this section we discuss how the inclusion of both the quartic effects in deriving slant TEC from FORTE-LAPP data and the Earth's curvature effects in converting the slant TEC to the vertical TEC (see Appendix B for a description) can correctly improve data agreement.

[47] Figures 14a and 14b show how including both the quartic and the curvature effects can correctly improve data agreement for slant distance greater than 2000 km (elevation angle less than about 24°) during daytime (0800–1700 LT) and during nighttime (2000–0500 LT) of a low solar activity year (1998), respectively. During daytime, including curvature effect only actually amplifies the positive biases existing in the case of neglecting both effects while the combined quartic and curvature effects effectively removes the biases. During nighttime, including curvature effect only produces the same magnitude of positive biases rather than negative biases existing in the case of neglecting both effects while the

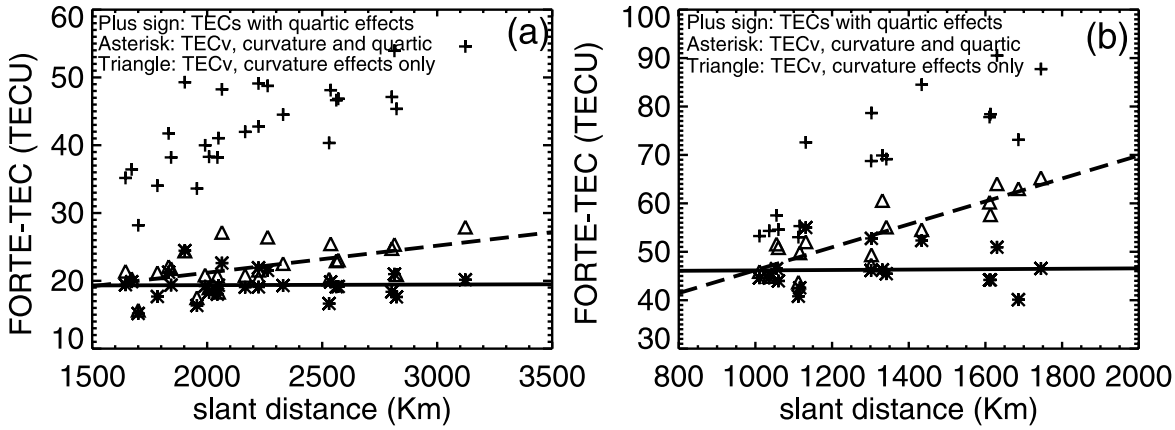

Figure 15. Curvature and quartic effects on FORTE-derived TECs for (a) 7–10 August 2000 and (b) 21–23 February 2001. Pluses represent slant TEC with quartic effects, triangles and the dashed line represent vertical TEC with curvature effect, and asterisks and the solid line represent vertical TEC with both curvature and quartic effects.

combined quartic and curvature effects result in an almost no bias linearly fitted line.

[48] To illustrate the improvement of data agreement with both the quartic and the curvature effects included for high solar activity years, we re-examined the two cases shown in Figures 11 and 12. Figures 15a and 15b show the slant FORTE TECs derived with the quartic effects included (pluses), the vertical TECs with curvature effects only (triangles), and the vertical TECs with both quartic and curvature effects included (asterisks) for the two cases given in Figures 11 and 12, respectively. We can see that including only the Earth's curvature effect results in larger biases than using the simple "plane-parallel" model, however, when quartic effects are included at the same time, the data agreements are correctly improved although there are still "residual" biases left in the two cases.

[49] In calculating the curvature effects, a mean value has to be assumed for the peak electronic density height (*hF*2). In fact, the peak electronic density height can vary from 200 km to 500 km. Our examinations found that the use of a reliable real-time *hF*2 may further improve data agreement. In the case of February 2001, the observed values of *hF*2 at Boulder (the ionosonde station closest to Los Alamos) range from 236 km to 251 km. It is interesting to find that the use of the "real-time" averaged *hF*2 of 240 km has virtually removed the "residual" biases. In the case of August 2000, the observed values of *hF*2 at Boulder vary from 284 km to 320 km, which gives an averaged value very close to 300 km. In fact, the biases in the case of August 2000 are negligibly small.

[50] Therefore, although the results in our FORTE-TEC analysis are little affected by applying the simple "plane-parallel" model in converting slant to vertical TEC to the first-order TEC, that is, neglecting both quartic and the curvature effects, we need to point out that the correct data agreement can only be achieved by including both the curvature and the quartic effects. Also important to point out is that the reliable "real-time" peak electronic density height must be taken into account in the curvature effects for specific event.

3.2.4. Effects Due to Thin-Shell Assumption

[51] In using the "thin shell" approximation (Appendix B), the model transforms the variation of the ionosphere's electron density distribution into an impulse function in the radial direction, creating a vertically equivalent ionosphere that varies as a function of shell height and the elevation angle of the line of sight from receiver to satellite. In this study we assumed a constant shell height of 350 km (*Hm*).

[52] We examined the effects on the resultant vertical TEC from using a larger *Hm* of 550 km, and a smaller *Hm* of 150 km compared to the mean *Hm* of 350 km. Figures 16a and 16b give the differences in absolute TEC between *Hm* = 350 km and *Hm* = 550 km (asterisks) and those between *Hm* = 350 km and *Hm* = 150 km (triangles) for daytime peak TEC period (1200–1400 LT) and nighttime (2000–0600 LT), respectively. We can see that the absolute differences in the estimated vertical TEC are generally smaller than 5 TECU during peak TEC daytime and smaller than 2 TECU during nighttime. The magnitude of the absolute differences in TEC decreases with increases in elevation angle, especially for nighttime. Further examinations indicate that on average the relative changes in the vertical TEC estimation are about 5–7% for both daytime and nighttime with respect

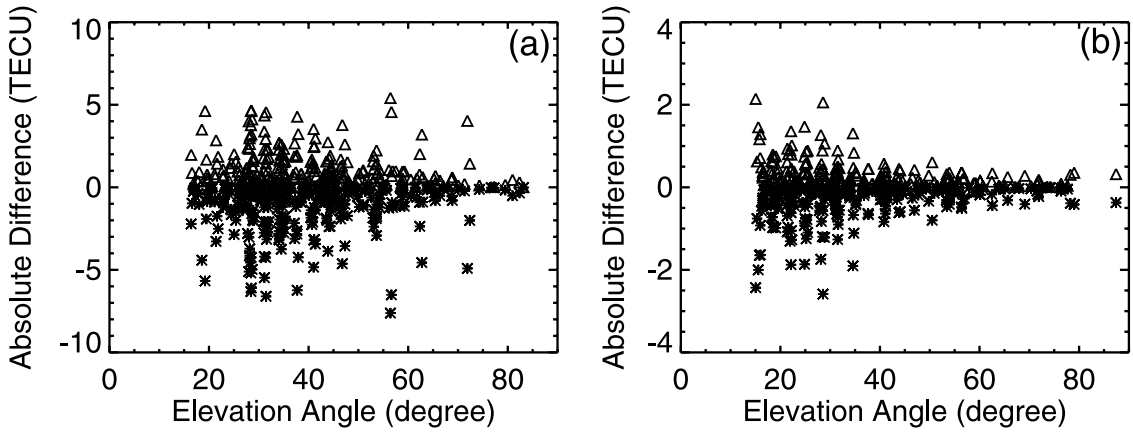

Figure 16. Differences in absolute TEC between *Hm* = 550 km (asterisks) and 150 km (triangles) with respect to default value *Hm* = 350 km as a function of elevation angle (>15°) for (a) daytime 1200–1400 LT and (b) nighttime 2000–0600 LT.

to the TEC values estimated with *Hm* = 350 km (Figures 17a and 17b).

[53] While a thin shell model is not a bad assumption if the elevation angle is not too low, such a conversion can introduce errors at low elevation angles when there are strong horizontal gradients in the ionosphere. Strong horizontal gradients may occur in the ionosphere over longitudes spanning different local time periods and in latitudes where strong electromagnetic disturbances modify the local solar produced ionosphere. Previous research indicates that severe gradient effects can result in a failure to capture true quantitative patterns, however, slant measurements through and outside regions of large gradients do portray the basic geophysical morphologies [e.g., *Mendillo et al.*, 1974]. In any case, no simple algorithm is currently available to take these gradient effects into account in conversions from slant to vertical TEC without invoking very sophisticated modeling. Thus employing the "horizontal uniformity" assumption for individual satellite-to-receiver ray paths remains the standard approach to derive the local ionospheric TEC.

[54] The error in the estimation of vertical TEC from slant TEC introduced by assuming a thin shell model has been reported in the literature only in a qualitative way. The possible dependence of this error on satellite elevation angle, satellite azimuth, ground station latitude, solar activity and season has been examined by comparative study using a 3-D ionospheric electron density model [*Radicella and Nava*, 2002]. On the basis of their results, our TEC values may be most affected because of thin shell assumption under three conditions: (1) during high

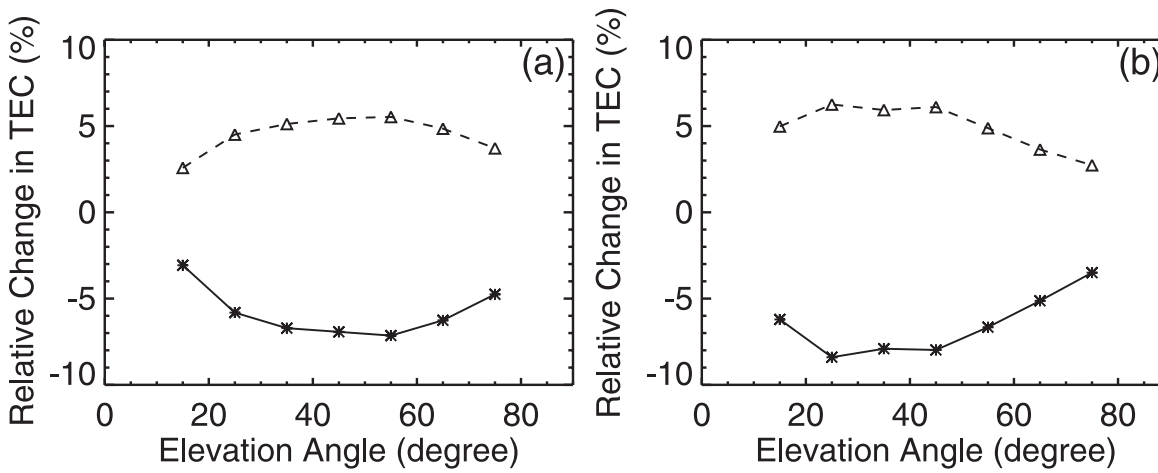

Figure 17. Same as Figure 16, but for relative TEC change (%).

Table 2. Storm-Time and Nonstorm-Time TECs for Selected Geomagnetic Storms From November 1997 to May 2002

Storm	Storm Date	Storm Category	Storm-Time TEC, TECU	Nonstorm-Time TEC, TECU	Time Interval, LT	Relative Changes, %
1	22–23 Nov 1997	large	20.2	10.4	1228–1318	95
2	17–18 Feb 1998	medium	12.8	11.3	1702–1735	13
3	10–11 March 1998	medium	22.0	5.8	1210–1302	279
4	2–5 May 1998	major	12.6	14.1	1508–1556	−11
5	6–7 Aug 1998	large	8.96	8.8	1915–1927	2
6	7–9 Nov 1998	large	62.4	30.1	0847–0921	107
7	18–19 Feb 1999	large	27.1	17.0	1120–1148	59
8	16–17 April 1999	medium	18.0	11.9	1126–1217	51
9	13–16 July 2000	major	26.1	23.7	1002–1042	10
10	10–13 Aug 2000	major	10.5	14.1	0549–0640	−26
11	31 March 2001	major	69.2	44.9	1202–1243	54
12	11–12 April 2001	major	39.3	38.9	0900–1127	1
13	6–7 Nov 2001	major	65.2	62.9	1232–1337	4

solar activity (2000–2002), (2) for the cold season (September–April), and (3) at low elevation angles.

[55] The uncertainty issues related to the thin shell assumption, as well as the quartic effects, can only be effectively resolved by very sophisticated modeling techniques, such as ray tracing. While such techniques require information about the electron density vertical profiles, the FORTE measurements of frequency-dependent time delay allow us to develop approaches to extract averaged ionosphere parameters which can be used as a starting point for developing advanced techniques. By separating the time delay caused by TEC dispersion (quadratic) and the time delay due to refractive bending and high-order electron profile terms (quartic) from the FORTE frequency-dependent time delays, it is possible to extract ionospheric peak electron density and effective slant thickness of the ionosphere. The effective slant thickness for the ionosphere can be determined given several measurements for various zenith angles of a broadband pulse and fitting the ratio of quartic to quadratic time delay at a fixed frequency [*Roussel-Dupré et al.*, 2001, equation 16]. The peak electron density can be obtained by taking the ratio of the slant TEC to the computed slant thickness of the ionosphere.

3.2.5. Geomagnetic Storm Effect

[56] In addition to the above technique-related uncertainties in deriving TEC, geomagnetic storms can cause large-scale enhancements and large amplitude fluctuations in TEC. At midlatitudes, the steep spatial gradients in TEC and the occurrence of strong radio scintillation have been observed over the continental United States during strong magnetic storms of the current solar cycle [e.g., *Steven et al.*, 1998; *Vo and Foster*, 2001]. The storm time characteristics of TEC variations at Tokyo (35.65°N, 139.54°E) have been investigated from GPS dual frequency signals for the 11 storms for 1997–1998 [*Yamamoto et al.*, 2000]. It has been shown that the TEC variation tends to increase during the first 24 hours of storm and then decrease below its usual day level with recovery in one or two days later. In this section, we examine geomagnetic storm effect on TEC variations at Los Alamos.

[57] To identify magnetic storm conditions during the period from November 1997 to July 2002, we use the criteria based on the 3-hour *Kp* index [*Gosling et al.*, 1991]. A "major" storm has a maximum $Kp \geq 8-$, together with a $Kp \geq 6-$ for at least three 3-hour intervals in a 24-hour period. A "large" storm is similar but has a maximum $7- \geq Kp \geq 7+$. A "medium" storm has a maximum $6- \geq Kp \geq 6+$, together with $Kp \geq 5-$ for at least three 3-hour intervals in a 24-hour period. For the identified storms, we search for FORTE TEC data availability within several days of the peak storm time. Because of the FORTE TEC data are limited time observations, we can only analyze possible storm effects during a certain time interval for a given storm. Therefore we identify the time interval where the TECs are available for each selected storm and compute storm-time and nonstorm-time TEC. Considering the general characteristics of TEC variations associated with a geomagnetic storm, storm time TEC values are defined as the averages over a time interval, usually up to one hour (to eliminate diurnal cycle factor), during storm time and the following 24-hour period. On the other hand, the nonstorm-time TEC values are evaluated on the averages during the same time interval at the closest dates before and after the storm, usually within three days. For comparison purposes, the diurnal cycle has to be removed. For example, we have storm-time TEC for 1000–1100, we may use nonstorm-time data for 0900–1200 LT to estimate TEC values at 1000–1100 if no nonstorm-time data are available for 1000–1100.

[58] Table 2 gives results of storm time and nonstorm-time-averaged TEC comparisons for the 13 selected storms during the FORTE data period, showing absolute

magnitude differences and relative changes with respect to normal conditions in TEC due to geomagnetic storm impact. Also given in Table 2 are the date of storm occurrence, storm category, and the time interval where the average TECs are computed.

[59] Our analyses indicate that the overall impact of geomagnetic storm on TEC variations at Los Alamos is characterized by an enhancement during the extended storm time (storm time plus 24 hours after). Out of the 13 selected storms, TEC enhancements occurred for 11 storms and TEC reductions happened for two storms. Note that the two storms with TEC reductions are the ones with several consecutive storms lasting for 3–4 days, the storm-time average TECs for these two cases computed over a period where the phases of storm-induced TEC increase-decrease fluctuations from the combined impacts of the consecutive storms may be canceled out. A previous study [*Yamamoto et al.*, 2000] indicates that during a negative value phase of the TEC variation, the TEC amplitude shows a remarkable reduction in summer compared to that in winter. We noticed that the two reduction cases happen to occur in summer time when the TEC reduction after 24 hours is large, making it possible for combined TEC reduction outcomes. Therefore, in most cases, we see overall enhancements in TEC as a result of geomagnetic storm impact at Los Alamos.

[60] The relative enhancements in TEC due to a geomagnetic storm at Los Alamos can reach as high as threefold of the normal TEC values. The magnitude of TEC enhancements is diversified over all storm categories without a clean-cut relationship between the storm intensity and the TEC enhancement. The three storms with the largest impact of twofold to threefold TEC enhancements (1, 3, and 6) are not the strongest ones as we would assume, but are medium to large ones. The three storms occurred in low solar activity years (1997 and 1998). The three storms with second significant TEC enhancements of larger than 50% (7, 8, and 11) are all single storms and cover storm categories from medium to major. The evaluations for these three storms are made during the peak TEC time interval (1100–1300) in the spring high TEC phase (February to April) of the seasonal cycle. The TEC enhancements for the remaining storms (2, 5, 9, 12, and 13) are all less than 15%. These storms also cover all the three storm categories with three out of five being major storms.

[61] The overall absolute enhancements in TEC at Los Alamos are up to about 30 TECU for the current half solar cycle. It is interesting to see how our results can be quantitatively compared with other storm case TEC studies. A storm case TEC study [*Basu and Basu*, 2002] found an increase and decrease of TEC between 20 and 40 TECU at Westford, Massachusetts (42.6°N, 71.5°E) for the storm occurring on 5 March 2001. We do not have the same storm case to compare against. Instead, our results for the 31 March 2001 storm case suggest an overall enhancement in TEC of about 25 TECU, or rather close agreement with the Westford case given that the TEC enhancements in our study are averages in nature while those in Basu and Basu's study are transient.

[62] Our study on the geomagnetic storm effects on TEC variations at Los Alamos may suggest that the storm effects can cause dramatic TEC enhancement as high as twofold to threefold. However, the effects are also complicated given that no clean-cut relationship may be derived between the storm intensity and the magnitude of TEC enhancement. For larger TEC enhancement the responsible storm does not have to be stronger. In particular, when two to three consecutive strong storms occurred in a row, since major enhancement usually occurs after about 24 hours following storm peak, a net TEC reduction may be seen because of the combination of the opposite phases in the TEC fluctuations due to storm effects. Although the geomagnetic storm effect can cause TEC variations as large as a factor of 3, the timescale of the effect is on the order of hours and the frequency and probability for such effects to occur are low; hence the effect on averaged TEC variability is small.

[63] It is noted that *Dst* index has been usually used to characterize the development of a geomagnetic storm for its finer temporal resolution [e.g., *Gonzalez et al.*, 1994]. We conducted a correlation study between *Kp* index and the *Dst* index (averaged over 3 hours) and found that for the time period in this study, the two indices are correlated at 50–60% consistently for daytime, nighttime, warm/cold season, and for low/high solar activity. Given the fact that this study estimates the averaged storm effects and does not deal with transient time-varying effects for a particular storm, we believe that the use of *Kp* instead of *Dst* does not affect the results to an extent that is discernible.

4. Summary

[64] The TEC variability at Los Alamos on diurnal, seasonal, interannual timescales and 27-day solar cycle is obtained from FORTE data analysis for the period of 1997–2002. Table 3 summarizes the TEC variability at Los Alamos on the basis of FORTE data analysis. The TEC variability features a significant diurnal cycle ranging from an early morning low to an early afternoon high by a factor of 5–7. A well-developed semiannual seasonal cycle is observed with two comparable peaks in March and October–November, respectively, and a major low in summer from May to August. On daily averaged monthly mean, the TEC seasonal cycle varies from low phase to peak phase by a factor of 50–100% while a twofold to threefold variation has been found in

Table 3. Total Electronic Content Variability (1997–2002) at Los Alamos

	Diurnal Cycle	Seasonal Cycle	11-Year Solar Cycle	27-Day Solar Cycle
Peak phase	0300–1400 LT	March; Oct–Nov	solar maximum	solar maximum
Lowest phase	0300–0400 LT	May–Aug	solar minimum	solar minimum
Amplitude	low solar phase, 3–21 TECU; high solar phase, 10–45 TECU	daytime,[a] 20–30 TECU; nighttime, 7–14 TECU	daytime, 10–50 TECU; nighttime, 5–20 TECU	SSN[b] 125–200, 20–50 TECU; SSN 160–260, 15–30 TECU
Day-to-day variations	10 to 30% (relative to mean values)	—	—	—
Storm effects	50 to <300% (relative to nonstorm mean)	—	—	—

[a]Daily averaged monthly means: 25–60 TECU for 4-hour averaged TECs during 1000–1400 LT.

[b]SSN: sunspot number.

the TEC seasonal cycle for the peak time period (1000–1400). The TEC variability on an 11-year solar cycle timescale is also significant. The monthly mean TEC values have increased by a factor of 4–5 from low solar activity years to high solar activity years. The TEC also varies on a 27-day solar cycle by a factor of 2–3.

[65] In addition to solar-related variability, random variations on day-to-day changes or as a result of geomagnetic storms also contribute to observed TEC variability at Los Alamos. The day-to-day random variation ranges from 10–30% of the mean TEC values while the changes due to geomagnetic storm effects can cause a TEC increase by 50–300%.

[66] Our study indicated the importance of quartic effects in deriving TEC from the VHF broadband signal data. However, we found that the quartic effect on transionospheric VHF radio signal propagation in deriving slant TEC and the Earth's curvature effect in converting the slant TEC to vertical TEC oppositely affect the TEC estimations and should be considered at the same time. Furthermore, the use of a real-time peak electronic density height may not make large differences in deriving averaged features but can become important in predicting accurate TEC for a specific date and time. Therefore a reliable peak electronic density height from ionosonde observations or from ionospheric model predictions is required for better TEC predictions.

[67] The significant while less investigated effect of geomagnetic activity on TEC variations due to a lack of data is an important issue that must be addressed for reliable TEC predictions. We have undertaken TEC observations using local GPS receivers in collaboration with researchers in LANL's GPS measurement team to obtain finer resolution data for geomagnetic storm and solar flare events for the purposes of investigating TEC variability on minute timescales, which is not possible using the FORTE data.

[68] Finally, we wish to expound on the future application of this technique of broadband VHF TEC determination. For example, are we proposing a constellation of satellites with broadband receivers to monitor the global TEC on a continuous basis? What are the advantages and limitations of such a system? Are we planning to field impulsive EMP generators globally to provide the source signal or can we use lightning for that purpose? What properties of the ionosphere can we reliably report, for example, TEC, peak ionospheric density, nominal radial extent of the ionosphere, scintillation index, coherence bandwidth?

[69] A proposal presently under review at Los Alamos and other U.S. government facilities involves development of an operational satellite-based radio frequency global lightning and storm tracking system. Such a system would most likely employ a constellation of geosynchronous or Global Positioning System (GPS)-

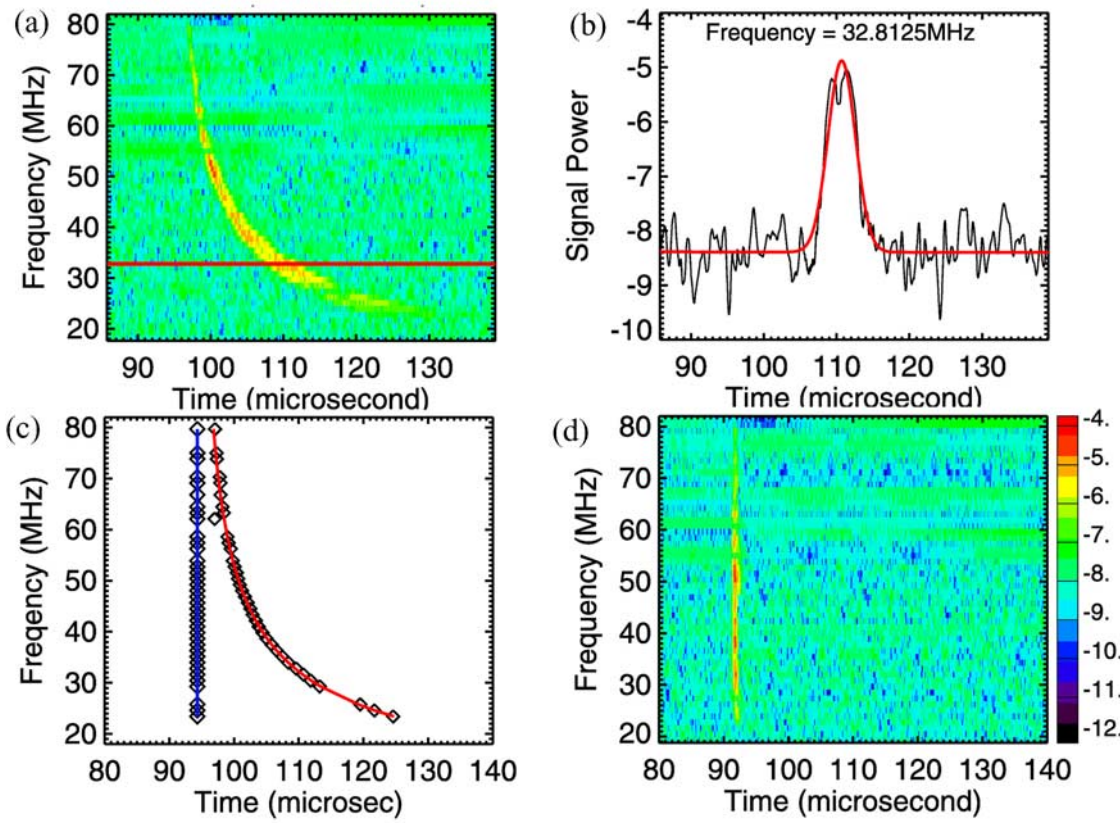

Figure A1. (a) Denoised FFT spectrogram. The red line is drawn at frequency 32.8125 MHz. (b) Signal power at 32.8125 MHz (black line) and its Gaussian fit curve (red line). (c) Polynomial function fit (the "chirped line" in red) with the first-order TEC effects and the quartic effects removed (vertical blue line). (d) Final signal power spectrogram after first-order TEC is dechirped, quartic delay is shifted, and fast mode is removed.

based broadband radio receivers. The receivers would ideally operate in the VHF (30–300 MHz) in order to allow detection of those frequency components of the signal that propagate through the ionosphere without reflection.

[70] The operational goal of such a system is to accurately geolocate, track, and report lightning events on a global basis. Geolocation accuracy however is strongly dependent on the ability to time tag the arrival of the signal at four or more satellites (with varying ionospheric paths) and to remove the ionospheric temporal delays. Therefore validation of the dispersion-removing technique used in this study to deduce the line-of-sight TEC from VHF signals has potentially huge significance for such an application. At the same time, a satellite-based global lightning detection system of this type could also provide global TEC measurements during the lightning season dependent only upon the occurrence of a detectable lightning event [e.g., *Pongratz et al.*, 2002]. Estimations of peak ionospheric density and nominal radial extent of the ionosphere would also be made possible by applying the approach described by *Roussel-Dupré et al.* [2001] to the power spectrogram of detected lightning signals. Furthermore, the scintillation index and the associated coherence bandwidth can be estimated on the basis of the thin phase screen approximation in solving the ionospheric transfer function for wide bandwidth signal propagation through ionization irregularities [*Knepp*, 1982], using the information about the frequency-dependent mean time delay and time delay variances of detected lightning signals.

[71] A concept definition has been proposed to use a constellation of VHF radio receivers aboard the upcoming Block IIF/III Global Positioning System (GPS) satellite constellation to monitor VHF lightning emissions on a global and continual basis [*Suszcynsky et al.*, 2000, 2001]. A constellation of FORTE-like receivers has been scheduled for launch beginning in 2006, which

is expected to be a powerful proxy tool for detecting, geolocating, and reporting storm activity and strong convection on a global basis in near real time [*Suszcynsky et al.*, 2005]. In another paper (Huang and Roussel-Dupré, submitted manuscript, 2005), we will present results of comparisons between the FORTE-derived TEC and the TECs from other sources.

Appendix A: Approach for Deriving Line-of-Sight TEC Using FORTE Data

[72] An approach is developed for deriving line of sight TEC and quartic effects using FORTE-received LAPP VHF signal data. A step-by-step description is given here using one of the LAPP events (Event time 8 November 1997, 2215:00.002961 UT; FORTE location 36.88°N, 103.037°W, 817.710 km; receiver HUMR).

[73] 1. For a given signal time series, perform a sliding window Fourier transform (FFT) and produce a power spectrogram; then the FFT spectrogram is filtered to suppress CW interference carriers (Figure A1a).

[74] 2. Determine peak power profile using a Gaussian curve fitting for each frequency window of the spectrogram. Figure A1b plots the signal power at 32.8125 MHz and its Gaussian fit curve.

[75] 3. Fit the peak power profile to a polynomial function of time delay, τ, and frequency, f:

$$\tau = a \times f^{-2} + b \times f^{-4} + c$$

Figure A1c plots the polynomial function with fitted coefficients a, b, and c (the "chirped line"). Also shown is a vertical line with the first-order TEC effects and the quartic effects removed.

[76] 4. From the coefficients of the polynomial function, extract TEC (coefficient a) and quartic delay term (coefficient b) and perform TEC only dechirp. The TEC only dechirped spectrogram shows the splitting at low frequencies, a result from the slow mode and the fast mode splitting due to magnetic field effects.

[77] 5. Remove the slow mode and determine peak power profile of the fast mode using Gaussian curve fitting and fit it to a second-order polynomial function of frequency

$$\tau = b \times f^{-4} + c,$$

then derive adjusted quartic delay and do a quartic delay phase shift. Note that there is still a residual chirp at the bottom of frequency band.

[78] 6. From the TEC dechirped and quartic delay phase shifted spectrogram, do one more polynomial fit to

$$\tau = a \times f^{-2} + b \times f^{-4} + c$$

and derive TEC and quartic delay "correction" coefficients and do corrective phase shift. Finally, a perfect vertical peak power profile is obtained (Figure A1d) which gives us a reliable TEC estimation as well as the magnitude of quartic effects.

Appendix B: Spherical Shell Model Relating Slant to Vertical TEC

[79] For a given ray from a transmitter to a receiver that intersects the ionosphere at a nominal peak electron density height, the spherical shell model relating slant TEC (*TECs*) to vertical TEC (*TECv*) at the ionospheric pierce point is given by

$$TECv = TECs \times \sin\delta$$
$$\sin\delta = \sqrt{1 - \left(\frac{\mathrm{Re} \times \cos\theta}{\mathrm{Re} + Hm}\right)^2},$$

where δ is the elevation angle at the ionospheric pierce point, θ is the local elevation angle at the ground transmitter/receiver (at LAPP in this study), Re is the radius of the Earth, and *Hm* is the height of the peak electron density above the Earth surface (350 km in this study).

[80] **Acknowledgments.** This work was performed under the auspices of the United States Department of Energy. We are indebted to Phil Klingner and Abram Jacobson for support in acquiring and working with FORTE data. We thank three anonymous reviewers for the depth of their analysis and commentary leading to the present version of this manuscript.

References

Arendt, P. R., and H. Soicher (1964), Downward electron flux at 1000 km altitude from electron content measurement at mid-latitudes, *Nature*, *204*, 984–985.

Argo, P. E., A. R. Jacobson, and S. O. Knox (1999), Geolocation of recurrent-emission lightning storms using the FORTE satellite, *Rep. LA-UR-99-4679*, Los Alamos Natl. Lab., Los Alamos, N. M.

Basu, S., and Su. Basu (2002), Effects of large magnetic storms on communication and GPS navigation systems at middle and equatorial latitudes, paper presented at 2002 General Assembly, Union Radio Sci. Int., Maastricht, Netherlands. (Available at hawk.iszf.irk.ru/URSI2002/GAabstracts/papers/p0534.pdf URSI)

Bent, R. B., and S. K. Llewellyn (1973), Documentation and description of the Bent ionospheric model, *Tech. Rep. AFCRL-TR-73–0657*, Air Force Cambridge Res. Lab., Hanscom Air Force Base, Mass.

Bilitza, D. (2001), International Reference Ionosphere 2000, *Radio Sci.*, *36*, 261–275.

Bilitza, D., and R. Williamson (2000), Towards a better representation of the IRI topside based on ISIS and Alouette data, *Adv. Space Res.*, *25*(1), 149–152.

Bilitza, D., K. Rower, and S. Pallaschke (1988), Study of ionospheric models for satellite orbit determination, *Radio Sci.*, *23*, 223–232.

Bilitza, D., C. Koblinsky, R. Williamson, and S. Bhardwaj (1998), Improving the topside electron density model for IRI, *Adv. Space Res.*, *22*(6), 777–792.

Conker, R. S., and M. B. El-Arini (2002), An ionospheric obliquity process responsive to line-of-sight azimuth and elevation, *Radio Sci.*, *37*(6), 1097, doi:10.1029/2002RS002615.

Davies, K., and G. K. Hartmann (1997), Studying the ionosphere with the Global Positioning System, *Radio Sci.*, *32*, 1695–1703.

Davies, K., W. Degenhardt, G. K. Hartmann, and R. Leitinger (1979), Comparison of total electron content measurements made with ATS-6 radio beacon over the U.S. and Europe, *J. Atmos. Terr. Phys.*, *42*, 411–416.

Doherty, P. H., and J. A. Klobuchar (1992), The effects of transmitter offsets on absolute TEC obtained from the GPS satellites, in *Proceedings of the International Beacon Satellite Symposium*, edited by M.-C. Lee, pp. 148–152, MIT Press, Cambridge, Mass.

Garcia-Fernandez, M., M. Hernandez-Pajares, J. M. Juan, J. Sanz, R. Orus, P. Coisson, B. Nava, and S. M. Radicella (2003), Combining ionosonde with ground GPS data for electron density estimation, *J. Atmos. Sol. Terr. Phys.*, *65*, 683–691.

Gonzalez, W. D., J. A. Joselyn, Y. Kamide, H. W. Kroehl, G. Rostoker, B. T. Tsurutani, and V. M. Vasyliunas (1994), What is a geomagnetic storm?, *J. Geophys Res.*, *99*, 5771–5792.

Gordienko, G. I., and S. N. Mukasheva (2001), Ionospheric response to the solar activity variation based on total electron content data, *Geomagn. Aeron.*, *41*(6), 766–770.

Gosling, J. T., D. J. McComas, J. L. Phillips, and S. J. Bame (1991), Geomagnetic activity associated with Earth passage of interplanetary shock disturbances and coronal mass ejections, *J. Geophys. Res.*, *96*, 7831–7839.

Jacobson, A. R., S. O. Knox, R. Franz, and D. C. Enemark (1999), FORTE observations of lightning radio-frequency signatures: Capabilities and basic results, *Radio Sci.*, *34*, 337–354.

Jakowski, N., S. Heise, A. Wehrenfennig, S. Schluter, and R. Reimer (2002), GPS/GLONASS-based TEC measurements as a contributor for space weather forecast, *J. Atmos. Sol. Terr. Phys.*, *64*, 729–735.

Knepp, D. L. (1982), Propagation of wide bandwidth signals through strongly turbulent ionized media, *Tech. Rep. DNA-TR-91–78*, 246 pp., Def. Nucl. Agency, Washington, D. C.

Ma, G., and T. Maruyama (2002), A comparison of GPS-derived TEC and *foF*2 over Japan, paper presented at 2002 General Assembly, Union Radio Sci. Int., Maastricht, Netherlands.

Massey, R. S., O. K. Stephen, R. C. Franz, D. N. Holden, and C. T. Rhodes (1998), Measurements of transionospheric propagation parameters using the FORTE satellite, *Radio Sci.*, *33*, 1739–1754.

Mendillo, M., J. A. Klobuchar, and H. Hajeb-Hosseinieh (1974), Ionospheric disturbances: Evidence for the contraction of the plasmasphere during severe geomagnetic storms, *Planet. Space Sci.*, *22*, 223–236.

Mosert de Gonzalez, M., and S. Radicella (1995), Study of ionospheric variability at fixed heights using data from South America, *Adv. Space Res.*, *15*(2), 61–65.

Pongratz, M. B., D. M. Suszcynsky, T. J. Fitzgerald, and A. R. Jacobson (2002), Passive, global, real-time TEC monitoring, *Eos Trans. AGU*, *83*(47), Fall Meet. Suppl., Abstract SA52A-0388.

Pulinets, S. A., and R. F. Benson (1999), *Radio-Frequency Sounders in Space: Review of Radio Sci.*, chap. 28, pp. 711–733, edited by W. R. Stone, Oxford Univ. Press, New York.

Pulinets, S. A., V. H. Depuev, A. T. Karpachev, S. M. Radicella, and N. P. Danilkin (2002), Recent advances in topside profile modeling, *Adv. Space Res.*, *29*(6), 815–823.

Radicella, S. M., and B. Nava (2002), Study of the obliquity factor error in slant to vertical and vertical to slant ionospheric delay conversion, paper presented at 2002 General Assembly, Union Radio Sci. Int., Maastricht, Netherlands. (Available at http://hawk.iszf.irk.ru/URSI2002/GAabstracts/papers/p1476.pdf)

Roussel-Dupré, R., A. R. Jacobson, and L. A. Triplett (2001), Analysis of FORTE data to extract ionospheric parameters, *Radio Sci.*, *36*, 1615–1630.

Schaer, S., G. Beutler, M. Rothacher, T. A. Springer (1996), Daily global ionosphere maps based on GPS carrier phase data routinely produced by the CODE Analysis Center, paper presented at IGS AC Workshop, Int. GPS Serv., Silver Spring, Md., 19–21 March.

Soicher, H. (1985), Variability of transionospheric signal time delay at high latitudes near solar minimum, in *AGARD Propagation Effects on Military Systems in the High Latitude Region*, *Rep. SEE N86–27531 18–32*, 9 pp., Army Commun. Electron. Command, Fort Monmouth, N. J. (Available at http://adsabs.harvard.edu/physics_service.html)

Steven, M., M. Cerry, and C. E. Dufton (1998), Total electron content changes in the ionosphere during the January 10, 1997 disturbances, *Geophys. Res. Lett.*, *25*, 3055–3058.

Suszcynsky, D. M., A. Jacobson, J. Fitzgerald, C. Rhodes, E. Tech, and D. Roussel-Dupré (2000), Satellite-based global lightning and severe storm monitoring using VHF receivers, *Eos Trans. AGU*, *81*(48), Fall Meet. Suppl., Abstract A6D-11.

Suszcynsky, D. M., S. Davis, A. Jacobson, M. Heavner, and M. Pongratz (2001), VHF global lightning and severe storm monitoring from space: Storm-level characterization of VHF lightning emissions, *Eos Trans. AGU*, *82*(47), Fall Meet Suppl., Abstract AE12A-0075.

Suszcynsky, D. M., A. R. Jacobson, J. Linford, T. E. Light, and A. Musfeldt (2005), VHF lightning detection and

storm tracking from GPS orbit, paper presented at 85th American Meteorological Society Meeting, San Diego, Calif., 9–13 Jan.

Tierney, H. E., A. R. Jacobson, W. H. Beasley, and P. E. Argo (2001), Determination of source thunderstorms for VHF emissions observed by the FORTE satellite, *Radio Sci.*, *36*, 79–96.

Tsai, H. F., J. Y. Liu, W. H. Tsai, C. H. Liu, C. L. Tseng, and C. C. Wu (2001), Seasonal variations of the ionospheric total electron content in Asian equatorial anomaly regions, *J. Geophys. Res.*, *106*, 30,363–30,369.

Vo, H. B., and J. C. Foster (2001), A quantitative study of ionospheric density gradients at mid-latitudes, *J. Geophys. Res.*, *106*, 21,555–21,563.

Wan Hassan, W. S., A. F. M. Zain, A. G. Ramli, H. Y. Hwa, and M. Abdullah (2002), Studies on equatorial total electron content near solar maximum activity from 1998–2000, paper presented at XXVIIth General Assembly, Union Radio Sci. Int., Maastricht, Netherlands. (Available at http://www.ursi.org/Proceedings/ProcGA02/ursiga02.pdf.)

Yamamoto, A., Y. Ohta, T. Okuzawa, S. Taguchi, I. Tomizawa, and T. Shibata (2000), Characteristics observed at Chofu for geomagnetic storms, *Earth Planets Space*, *52*, 1073–1076.

Z. Huang and R. Roussel-Dupré, Atmospheric, Environmental and Climatic Dynamics Group, Earth and Environmental Sciences Division, Los Alamos National Laboratory, Los Alamos, NM 87545, USA. (zhen_huang@lanl.gov)